



#### Available online at www.sciencedirect.com

# **ScienceDirect**

Geochimica et Cosmochimica Acta 271 (2020) 132-153

# Geochimica et Cosmochimica Acta

www.elsevier.com/locate/gca

# Decoupling feldspar dissolution and precipitation rates at near-equilibrium with Si isotope tracers: Implications for modeling silicate weathering

Chen Zhu <sup>a,\*</sup>, J. Donald Rimstidt <sup>d,1</sup>, Yilun Zhang <sup>a,b</sup>, Jinting Kang <sup>a,f</sup>, Jacques Schott <sup>e</sup>, Honglin Yuan <sup>c</sup>

a Department of Earth and Atmospheric Sciences, Indiana University, Bloomington, IN 47405, USA
 b Doctoral Program in Environmental Science, Indiana University, Bloomington, IN 47405, USA
 c Northwest University, State Key Laboratory Continental Dynamics, Department of Geology, Xi'an 710069, China
 d Department of Geological Sciences, Virginia Tech, Blacksburg, VA 24061, USA
 c Géosciences Environnement Toulouse, CNRS-UPS-OMP, 14 av. Édouard Belin, 31400 Toulouse, France
 f CAS Key Laboratory of Crust-Mantle Materials and Environments, School of Earth and Space Sciences, University of Science and Technology of China, Hefei 230026, China

Received 12 August 2019; accepted in revised form 19 December 2019; Available online 27 December 2019

#### Abstract

Here we show that the isotope tracer experimental method for kinetic studies, aided by the recent advance and accessibility of multi-collector inductively coupled plasma mass spectrometry (MC-ICP-MS) analysis for non-traditional stable isotopes, can provide *unidirectional dissolution rates* at near-equilibrium conditions. For a long time, the only rates available at near-equilibrium were net reaction rates—dissolution rates minus precipitation rates. This is because the conventional experimental method of kinetic studies is based on element concentrations and can only provide net rates. The availability of unidirectional rates allows us to re-examine some fundamental concepts and practices of modeling weathering in geochemistry.

In this study, we used the  $^{29}$ Si isotope tracer to conduct albite and K-feldspar dissolution experiments at near-equilibrium conditions in near-neutral pH solutions at 50 °C. Results show that the saturation indices (SI) of solutions approached zero with respect to albite and K-feldspar after  $\sim$ 240–360 h (h), but  $^{29}$ Si/ $^{28}$ Si ratios of the experimental solutions indicated continual dissolution for another 720–1440 h. The rates of total Si precipitation were much smaller than the rates of Si dissolution. The experimental solutions were supersaturated with respect to amorphous Al(OH)<sub>3</sub>, gibbsite, quartz, allophane, imogolite, and kaolinite. The SI of the solutions remained constant with respect to these phases while Al concentrations slightly decreased and Si concentrations slightly increased, indicating the coupled feldspar dissolution and precipitation of secondary phases, such as albite  $\rightarrow$  amorphous Al(OH)<sub>3</sub> + quartz or albite  $\rightarrow$  solution + Al-Si phase(s), instead of significant albite and K-feldspar precipitation (the reverse reaction) at 50 °C. Reaction path modeling of the temporal evolution of Si, Al, Na, and pH revealed that albite dissolution (without significant backward reaction) coupled with the precipitation of a secondary phase with a Si:Al ratio of  $\sim$ 2:1 can successfully match the experimental data.

Given the negligible feldspar precipitation reactions in low-temperature systems (e.g.,  $T \le 100$  °C), we recommend modeling feldspar weathering using unidirectional forward rates together with secondary phase precipitation rates in near-equilibrium, feldspar-undersaturated systems. This can be accomplished with minor modifications in geochemical modeling software or input files. The coupled feldspar dissolution with secondary phase precipitation arrests the system in a

<sup>\*</sup> Corresponding author.

E-mail address: chenzhu@indiana.edu (C. Zhu).

<sup>&</sup>lt;sup>1</sup> Author passed away on March 24, 2019.

near-equilibrium steady state. Using affinity-based rate equations such the classical linear Transition State Theory rate law or the Burch empirical relation together with far-from-equilibrium rate data will predict significant feldspar precipitation in solutions undersaturated but close to equilibrium with respect to feldspars, which is unlikely at near ambient temperatures. © 2019 Elsevier Ltd. All rights reserved.

Keywords: Kinetics; Feldspar; Isotope doping; Near-equilibrium; Weathering; Carbon sequestration

#### 1. INTRODUCTION

It is generally believed that most reactions in geologic systems proceed at near-equilibrium conditions because geological and some environmental processes (e.g., CO<sub>2</sub> sequestration and nuclear waste disposal) span a timeframe from tens of thousands of years to millions of years (e.g., White, 1995; Schott et al., 2012). However, traditionally only far-from-equilibrium silicate reaction rates have been reliably measured under weathering conditions—that is, ambient temperature and near-neutral pH—because of the limitation of the *conventional experiment method* of kinetics studies, which relies on temporal changes of Si and/or Al concentrations.

Although the knowledge of *near-equilibrium* kinetics in various natural and engineered water-rock systems is critical to many societal problems and endeavors, a literature search found only 27 experimental studies for silicate minerals and basalt glass under *near-equilibrium* conditions in the last three decades. In contrast, there exist a large number of dissolution rates at *far-from-equilibrium*, and various temperature and pH conditions (See compilations by Palandri and Kharaka, 2004; Marini, 2007; Brantley et al., 2008; Marty et al., 2015).

This paucity of rate data under near-equilibrium conditions is mostly due to the conventional experimental method's inability to detect slow near-equilibrium reactions and to account for secondary phase precipitation. This is particularly true at near-neutral pH conditions, which is the condition for the majority of natural waters (Drever, 1988; McBride, 1994; Langmuir, 1997). For example, it is impossible to prepare a near-neutral pH solution that is near-equilibrium with respect to feldspars but not supersaturated with a large number of secondary Al-Si phases. Therefore, previous experiments that studied alkali feldspar dissolution rates at near-equilibrium conditions were performed at a pH near 9 (Fig. 1) where it is possible to prepare a solution avoiding considerable supersaturation with respect to common aluminum hydroxides and aluminosilicate phases.

The pioneering and meticulous experimental work to determine near-equilibrium feldspar reactions using the conventional experimental method (Burch et al., 1993; Gautier et al., 1994; Oelkers et al., 1994; Alekseyev et al., 1997; Berger et al., 2002; Alekseyev et al., 2004; Beig and Lüttge, 2006; Hellmann and Tisserand, 2006; Zhu et al., 2010; Pollet-Villard et al., 2016) helped to advance our understanding of this important geochemical kinetics subject. However, several competing hypotheses have been proposed to interpret the generally observed reduced net dissolution rates near-equilibrium, such as Al inhibition

(Oelkers and Schott, 1995; Schott and Oelkers, 1995), secondary phase precipitation (Alekseyev et al., 2004), and different reaction mechanisms at near- and far-from-equilibrium (Burch et al., 1993; Hellmann and Tisserand, 2006). Some experiments observed a "rate plateau" at far-from-equilibrium (Hellmann and Tisserand, 2006) while others did not (Gautier et al., 1994). New experimental methods and new types of data must be introduced to resolve these longstanding controversies.

It has long been recognized that isotopes can provide unique information to separate the forward from reverse reactions in biological studies (Melander, 1960; Melander and Saunders, 1979). In the 1990s, the isotope tracer method was applied with spikes of <sup>39</sup>K and <sup>84</sup>Sr for simultaneously measuring rates of dissolution of K-feldspar, biotite and plagioclase during the hydrothermal alteration of a granite in conditions close to equilibrium (Zuddas et al., 1995; Seimbille et al., 1998), and with <sup>84</sup>Sr/<sup>87</sup>Sr and <sup>44</sup>Ca/<sup>42</sup>Ca spikes for measuring rates of calcite recrystallization and conversion from aragonite to calcite (Beck et al., 1992). Gaillardet (2008) gave an excellent review of this method and pointed out its potential.

Recently, Si isotopes were successfully applied to measuring the forward dissolution reaction rate of albite at far-from-equilibrium (Gruber et al., 2014; Zhu et al., 2016), forward and backward reaction rates of quartz at equilibrium (Liu et al., 2016), and forward dissolution rates of kaolinite at near-equilibrium conditions (Gong et al.,

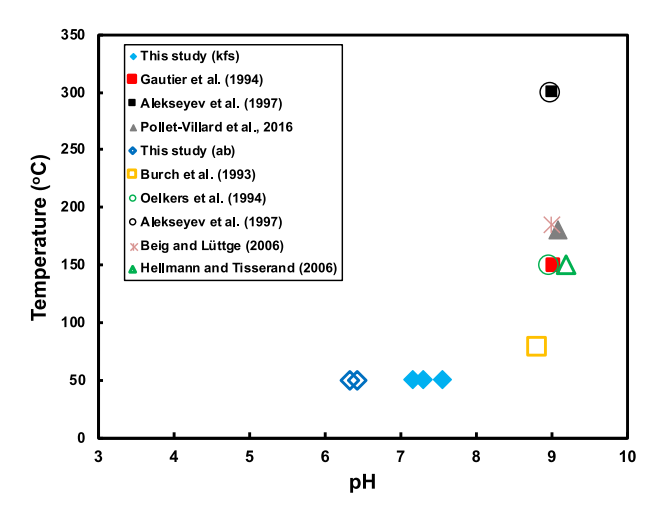


Fig. 1. Temperature and pH conditions of near-equilibrium dissolution experiments for albite and K-feldspar. Solid symbols denote K-feldspar experiments; open symbols albite experiments.

2019). This method immerses the mineral sample containing the naturally abundant <sup>28</sup>Si isotope in a solution enriched with the rare <sup>29</sup>Si isotope. By monitoring the rate of change of the solution's <sup>28</sup>Si/<sup>29</sup>Si ratio, it is possible to determine the rates of silica transfer from the mineral into the solution. Si isotope ratios in the solution samples are measured using high-resolution multiple-collector inductively coupled plasma mass spectrometry (MC-ICP-MS). Because the precipitation of the isotopes into secondary phases does not noticeably change the isotopic ratios of the fluids (the fractionation effect is negligible in heavily spiked systems), dissolution rates can still be measured when secondary phase precipitation takes place (Gruber et al., 2014; Zhu et al., 2016).

On other fronts, the use of the concept of forward and reverse reaction rates is commonplace in the field of isotope geochemistry (e.g., Weiss et al., 2013 for an introduction of isotope concepts). Recently, detailed models have been developed based on the Transition State Theory (TST) rate law to describe Ca isotope fractionation and trace metal partitioning during CaCO<sub>3</sub> precipitation (e.g., DePaolo, 2011 and refs therein). While isotope geochemistryoriented studies have focused on decoupling equilibrium and kinetic isotope fractionation effects based on the assumption that reaction rates are already known, our studies have aimed at obtaining the reaction rates themselves by making the isotope fractionation effects negligible in the experimental systems by overwhelming the system with rare isotope tracers. Furthermore, the Si isotope tracer method has also been used for studies of the dissolution mechanisms of silicate glasses (Geisler et al., 2010; Valle et al., 2010; Geisler et al., 2015; Gin et al., 2015; Verney-Carron et al., 2017). The combination of these approaches holds great promise for addressing different aspects of geochemical kinetics.

In this study, we used the Si isotope tracer method and conducted albite and K-feldspar dissolution at 50 °C and near-neutral pH. As opposed to the near-equilibrium experiments using the conventional method (Burch et al., 1993; Gautier et al., 1994; Oelkers et al., 1994; Alekseyev et al., 1997; Alekseyev et al., 2004; Beig and Lüttge, 2006; Hellmann and Tisserand, 2006; Zhu et al., 2010; Pollet-Villard et al., 2016), this study reports unidirectional forward rates of albite and K-feldspar dissolution at near-equilibrium conditions.

Below, we first present the experimental data from Si isotope tracer experiments. The experiments conducted for this study were performed in the pH range of 6.4–7.6 using solution compositions that are more representative of natural solutions. We then speculate as to appropriate approaches to modeling silicate weathering reactions.

# 2. BACKGROUND OF NEAR-EQUILIBRIUM KINETICS

Much of the discussion below is common knowledge to geochemists. However, these topics need to be revisited in the new light of the availability of unidirectional rates.

#### 2.1. Net reaction rates versus unidirectional rates

See Table 1 for symbols and definitions. For the convenience of discussion, here we follow the convention that near-equilibrium is defined as the region of  $\Delta_r G/RT > -5$  (Burch et al., 1993; Rimstidt, 2014) although this definition has the flaw that  $\Delta_r G$  values are related to how large the chemical formula for the mineral of interest is written. For the albite dissolution reaction at near-neutral pH,

NaAlSi<sub>3</sub>O<sub>8</sub> + 8H<sub>2</sub>O 
$$\stackrel{r_+}{\underset{r_-}{\rightleftharpoons}}$$
 Na<sup>+</sup> + Al(OH)<sub>4</sub><sup>-</sup> + 3H<sub>4</sub>SiO<sub>4</sub><sup>o</sup>(aq) (1)

the rates of albite dissolution by convention are based on Si flux:

$$r_{net} = r_{+} - r_{-} = \frac{1}{v \cdot S_A} \frac{d[SiO_2]}{dt}$$
 (2)

where  $r_+$  and  $r_-$  denote rates (mol albite m<sup>-2</sup> s<sup>-1</sup>) of the forward and reverse reactions, respectively. The net reaction rate,  $r_{\rm net}$ , (expressed in mol (ab) m<sup>-2</sup> s<sup>-1</sup>) is also often called the *overall rate*. v stands for the stoichiometric coefficient of Si in the silicate mineral of interest, e.g., 3 for albite.  $S_{\rm A}$  (m<sup>2</sup>/L) stands for the reactive surface area (Helgeson et al., 1984) or the concentration of the reactive surface sites (Stumm, 1992). However, in practice, these properties are currently inaccessible, and  $S_{\rm A}$  is approximated by either the Braunauer-Emmett-Teller (BET) or geometric surface area (Lasaga, 1998).

Theoretically, when a system approaches equilibrium, the thermodynamic drive diminishes, and the net reaction rate decreases.  $r_{\text{net}}$  is a function of  $\Delta_{\text{r}}G$  for an *elementary reaction* in accordance with the Principle of Detailed Balance if the forward and reverse reactions have the same mechanisms (Ohlin et al., 2009; Liu et al., 2016):

$$r_{net} = r_{+} - r_{-} = r_{+} (1 - e^{\Delta_{r}G/RT})$$
 (3)

Fig. 2 shows the relationships between  $r_+$ ,  $r_-$ ,  $r_{\text{net}}$ , and  $\Delta_r G$  (when all other conditions are the same). If the above assumptions and relationships hold,  $r_+$  should be independent of  $\Delta_r G$ ;  $r_-$  rises exponentially in the near-equilibrium region;  $r_{net}$  has a "plateau" at the far-from-equilibrium region but decreases exponentially when the experimental solutions approach equilibrium with respect to albite. In the very near-equilibrium region (e.g.,  $\Delta_r G \ge -RT$ , e.g., Nagy et al., 1991), rates decrease linearly with  $\Delta_r G$ , and thus this rate equation is sometimes called the "linear rate equation" (Burch et al., 1993). It should be noted that a relation similar to Eq. (3) is derived from Transition State Theory (Eyring, 1935) for an elementary reaction,  $r_{net} = r_+ (1 - e^{\Delta_r G/\sigma RT})$  where  $\sigma$ , the Temkin's stoichiometric number, is equal to the ratio of the rate of destruction of the activated complex—the high energy ground state species formed from reactants and in equilibrium to them to the overall reaction rate.

At equilibrium,  $r_+ = r_-$ , and  $r_{\rm net} = 0$ . In the far-from-equilibrium region, the reverse reaction is negligible (see Fig. 2,  $\Delta_r G < -5RT$ ). Hence,

$$r_{\rm net} \approx r_+$$
 (4a)

Table 1 List of symbols and definitions.

Symbol	Definition
$\Delta_{\rm r}G_i$	Gibbs free energy of the j <sup>th</sup> reaction (kJ/mol)
$\Delta_f G^{\rm o}$	The standard Gibbs free energy of formation $(kJ \text{ mol}^{-1})$
$\Delta_r H^{\circ}_T$	The standard enthalpy of reaction at temperature $T \text{ (kJ mol}^{-1})$
$\Delta_f H^{\circ}_T$	The standard enthalpy of formation at temperature $T(kJ \text{ mol}^{-1})$
$f_{28}$	<sup>28</sup> Si fractional abundance (0 to 1) in experimental solution $f_{28} = \left[\frac{28}{Si}\right] / \left(\left[\frac{28}{Si}\right] + \left[\frac{29}{Si}\right] + \left[\frac{30}{Si}\right]\right)$ ; $f_{28} = \frac{1}{1 + R_{29/28} + R_{30/28}}$ ; $R_{29/28}$ stands for the isotopic ratio; similarly for $f_{29}$ and $f_{30}$
$k_{+}$	Apparent forward rate constant of albite dissolution in mol (feldspar) m <sup>-2</sup> s <sup>-1</sup>
$k_{-}$	Apparent reverse rate constant of albite dissolution in mol (feldspar) m <sup>-2</sup> s <sup>-1</sup>
K	Equilibrium constant
R	Gas constant $(8.314 \mathrm{Jmol^{-1}K^{-1}})$
$r_{net} r_{\pm}$	Net or overall reaction rate in mol (feldspar) $\text{m}^{-2} \text{s}^{-1}$ ; $r_{net} = r_+ - r$
$\tilde{r}_{net}$	Apparent net rate in mol (feldspar) m <sup>-2</sup> s <sup>-1</sup> $\tilde{r}_{net} = r_+ - r r_{2nd}$
$r_{+}$	Forward rate of feldspar dissolution in mol (feldspar) m <sup>-2</sup> s <sup>-1</sup>
$r'_+$	Forward rate of feldspar dissolution in mol (feldspar) L <sup>-1</sup> s <sup>-1</sup> ; $r'_{+} = r_{+} \cdot S_{A}$
$r_{-}$	Reverse rate of feldspar dissolution reaction (precipitation or formation) in mol (ab) $m^{-2}$ s <sup>-1</sup> ; similarly, for $r'_{-}$
$r_{2nd}$	Precipitation rate of secondary mineral in mol (Si) m <sup>-2</sup> s <sup>-1</sup> ; similarly, for r' <sub>2nd</sub>
r'pre	$r'_{\rm pre} = vr'_{-} + r'_{\rm 2nd}$ , defined as "precipitation rate" in mol L <sup>-1</sup> s <sup>-1</sup>
r'pre,Si	The total Si precipitation rate (mol Si $L^{-1}$ s <sup>-1</sup> )
r'pre,Al	The total Al precipitation rate (mol Al $L^{-1}$ s <sup>-1</sup> )
$S_{\rm A}$	Surface area load of feldspar (m <sup>2</sup> /L) in the reactor; $S_A = s_A * m/V$ , where m denotes the mass (g) of reactant, V the volume of
	solution in the reactor, and $s_A$ the specific surface area (m <sup>2</sup> /g). e.g., 0.143 m <sup>2</sup> /g*1.0 g/0.01L for albite
$S_T^{\text{o}}$	The standard molar entropy at temperature $T(J \text{ mol}^{-1} \text{ K}^{-1})$
T	Temperature (K)
t	Time (s)
$\Delta t$	Time interval from time $t$ to time $t + 1$
V	The volume of the solution in a reactor (L)
[X]	Total concentration of element or species X
[X]t	Total concentration of element or species $X$ at time $t$
$v_{ab}$	The stoichiometric coefficient in molecular formula of albite
$v_{\mathrm{pre}}$	The stoichiometric coefficient of the secondary precipitation phase
Abbrev*	
ab	Albite
anl	Analcime
am	Amorphous
aq	Aqueous species
kfs	K-feldspar
kln	kaolinite
pre	Precipitation
SI	Saturation index

<sup>\*</sup> Mineral abbreviations follow Siivola and Schmid (2007).

However, in the near-equilibrium region, the reverse reaction is no longer negligible. The net dissolution rate is related to  $\Delta_r G$  as shown in Eq. (3) and the blue dashed line in Fig. 2. The conventional experimental method, based on [Si] and occasionally [Al], measures

$$r_{\text{net}} = r_+ - r_- \tag{4b}$$

This method cannot measure  $r_+$  or  $r_-$ . Therefore, all the near-equilibrium dissolution rates available in the geochemical literature are  $r_{\text{net}}$ . The effects of the diminishing thermodynamic drive as the system approaches to equilibrium is expressed as reduced dissolution rates.

When a Si-containing secondary phase precipitates, the conventional experimental method actually measures the apparent net rate  $(\tilde{r}_{\text{net}})$  rather than the "true" net rate  $(r_{\text{net}})$ :

$$\tilde{r}_{\text{net}} = r_+ - r_- - r_{\text{2nd}} \tag{4c}$$

where  $r_{2\text{nd}}$  denotes the rates of Si-containing secondary phase(s) such as kaolinite, allophane, and amorphous silica, and  $\tilde{r}_{\text{net}}$ the apparent net rate. Therefore, all near-equilibrium rate data available in the literature are actually  $\tilde{r}_{\text{net}}$ , unless it could be verified that no Si-bearing secondary phase was precipitated.

Great care was taken in previous studies to verify possible secondary phase precipitation or the absence of it, but it was a challenge. The amount of material precipitated is small, usually too small for X-ray diffraction detection. Al/Si stoichiometry (i.e., 1:3 for albite dissolution) was commonly used for justifying the absence of precipitation of secondary phases, but was not always observed. The uncertainties of Si and Al analyses are large relative to their incremental changes. SEM was used to examine the reaction products, and usually found some precipitates (e.g., Burch et al., 1993; Hellmann and Tisserand, 2006), but

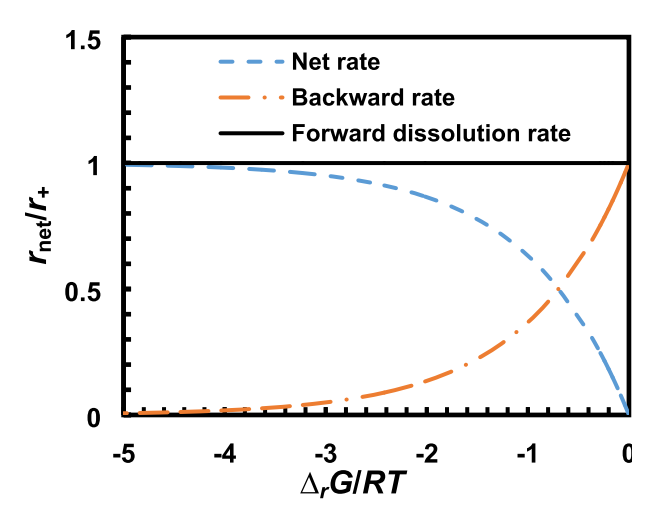


Fig. 2. A schematic graph to illustrate the relationships among net rate  $(r_{net})$ , forward dissolution rate  $(r_+)$ , and reverse rate  $(r_-)$  as described by Eq. (3) for an elementary reaction that obeys the Principle of Detailed Balance at equilibrium as well as at far-from-equilibrium. For rates in the discussion, all other conditions (pH, T, solution chemistry) are the same.

the amount of precipitates was deemed to be too small to affect calculated rates significantly. This interpretation was not universally accepted. For example, Alekseyev et al. (2004) asserted that the 1–2 orders of magnitude reduced dissolution rates near-equilibrium in Burch et al. (1993) were due to precipitation of secondary phases.

What is presented above can be called the "net rate paradigm." Because unidirectional rates  $r_+$  and  $r_-$  were previously not available, the only recourse available to geochemists was to seek functional relationships between the net rate  $(r_{\rm net})$  and Gibbs free energy of the reaction  $r_{\rm net} = f(\Delta_r G)$ . However, in Eq. (3), the  $\Delta_r G$  is the Gibbs free energy for the overall reaction, for example, R1. The form of  $f(\Delta_r G) = (1 - e^{\Delta_r G/\sigma RT})$  is only theoretically valid for an elementary reaction as the PDB demands. In order to use this form, it is generally assumed in the geochemical literature that there are numerous elementary reactions for the overall reaction such as Reaction (1), but only one elementary reaction is the rate-limiting step. Therefore,  $\Delta_r G^{overall}$  is equal to  $\Delta_r G^e$  (Nagy et al., 1991), where the superscript "e" denotes the elementary reaction.

Nagy et al. (1991) gave a detailed discussion of the conditions that must be met for the relationship  $f(\Delta_r G) = (1 - e^{\Delta_r G/\sigma RT})$  is applicable. To illustrate further the stringent conditions that must be met for this simplification, they used an example of two elementary reactions. From their examples, it is apparent that it is unlikely that the required conditions can be met for multi-oxide mineral dissolution reactions. Most geochemical kinetics papers also heeded similar words of caution for the use of Eq. (3) for overall reactions.

However, a number of experiments near-equilibrium have shown that the actual relationship between  $r_{\rm net}$  and  $\Delta_{\rm r}G$  deviates from Eq. (3). For feldspar dissolution, net rates are reduced at much more negative  $\Delta_{\rm r}G$  values than those predicted by Eq. (3) (further toward left in Fig. 2)

while the measured rates close to equilibrium are significantly slower than what Eq. (3) predicts.

Oelkers et al. (1994) and Gautier et al. (1994) explained these reduced dissolution rates within the framework of TST by the formation of aluminum-free precursor complexes controlling feldspars dissolution reaction or, in other words, by Al inhibition of dissolution.

Burch et al. (1993) used an empirical parallel rate law below to interpret their experiments of albite dissolution at 80 °C and pH 8.8,

$$r_{net} = k_1 \left( 1 - \left( e^{n\Delta_r G/RT} \right)^{m_1} \right) + k_2 \left( 1 - \left( e^{\Delta_r G/RT} \right)^{m_2} \right) \tag{5}$$

where  $k_1$  and  $k_2$  denote the rate constants in units of mol m<sup>-2</sup> s<sup>-1</sup>, and n,  $m_1$ , and  $m_2$  are empirical parameters fitted from experimental data (Zhu, 2009). Eq. (5) suggests two parallel mechanisms that operate separately under far-from-equilibrium and near-equilibrium conditions, respectively (Burch et al., 1993; Hellmann and Tisserand, 2006). Far from equilibrium, dissolution is driven by the nucleation at dislocation outcrops of etch pits that are the source of steps across the surface. Closer to equilibrium, below a critical Gibbs free energy value,  $\Delta G_{\rm crit}$ , etch pits stop nucleating and dissolution occurs only at pre-existing edges and corners at a much lower rate. The validity of Eq. (5) has been disputed by Lüttge (2006), who did not find a continuous function of  $\Delta_{\rm r}G$ , but instead found two Eq. (3) variants below and above the  $\Delta_{\rm r}G_{\rm crit}$  value.

It also must be noted that the majority of rate data compilations available in the literature are for far-fromequilibrium rates (e.g., Eq. (4a)). For example, Palandri and Kharaka (2004) compiled a database of essentially far-from-equilibrium rates. These rates must be extrapolated to near-equilibrium in order to model geochemical systems properly because geochemical reactions in natural systems mostly proceed at near-equilibrium conditions, given the long time span of most geological processes. Parrates with the relationship  $f(\Delta_r G)$ these  $= (1 - e^{\Delta_r G/\sigma RT})$  or its variants to get the near-equilibrium rate implicitly assumes that Eq. (3) for an elementary reaction is also valid for the overall reaction, and, within the TST approach, that the stoichiometry of the activated complex is the same as that of the dissolving mineral. Furthermore, in models of using this approach, a reduced dissolution rate implies feldspar precipitation in undersaturated solutions near-equilibrium. This paradigm, however, can change with the availability of unidirectional rates, as shown in this study.

### 2.2. A new type of feldspar reaction rates

Si isotope tracer experiments provide *unidirectional rates* of feldspar dissolution  $(r_+)$ .  $r_+$  is constant across solution saturation states (see the  $r_+$  line in Fig. 2) if the reaction mechanisms do not change. These rates were calculated from  $^{29}$ Si/ $^{28}$ Si ratios only (Zhu et al., 2016). Precipitation of Si-bearing secondary phases consumes Si, but changes the  $^{29}$ Si/ $^{28}$ Si ratios negligibly in experimental solutions, making this method applicable when secondary phases precipitate, such as in near-neutral pH solutions.

For a batch reactor system, considering both primary mineral dissolution and secondary phase precipitation, the temporal evolution of silica concentration and silicon isotope concentrations can be described with a set of mass balance equations (isotope fractionation due to both dissolution and precipitation has been neglected, Zhu et al., 2016):

$$\begin{cases} [Si]^{t+1} = (vr'_{+} - r'_{pre,Si})\Delta t + [Si]^{t} \\ [^{28}Si]^{t+1} = (vf_{28,kln}r'_{+} - f_{28,t}r'_{pre,Si})\Delta t + f_{28,t}[Si]^{t} \\ [^{29}Si]^{t+1} = (vf_{28,kln}r'_{+} - f_{29,t}r'_{pre,Si})\Delta t + f_{29,t}[Si]^{t} \end{cases}$$
(6)

where r' and r'<sub>pre</sub> are defined in Table 1. For a batch reactor with constant dissolution and precipitation rates, Eq. (5) is solvable analytically,

$$\begin{cases}
f_{28,t} = f_{28,ab} - (f_{28,ab} - f_{28,t0}) \left(\frac{v_{ab}r'_{+} - r'_{pre,Si}}{[Si]^{0}}t + 1\right)^{\frac{-v_{ab}r'_{+}}{v_{ab}r'_{+} - r'_{pre,Si}}} \\
f_{29,t} = f_{29,ab} - (f_{29,ab} - f_{29,t0}) \left(\frac{v_{ab}r'_{+} - r'_{pre,Si}}{[Si]^{t0}}t + 1\right)^{\frac{-v_{ab}r'_{+}}{v_{ab}r'_{+} - r'_{pre,Si}}} \end{cases} (7)$$

We now have two equations for two unknowns  $(r_+ \text{ and } r'_{\text{pre,Si}})$ . With the aid of Excel® solver, steady-state rates can be fitted to experimental data of  $f_{28}$ , and  $f_{29}$ ,. In practice,  $f_{28}$ , and  $f_{29}$ , are not sensitive to  $r'_{\text{pre,Si}}$  unless the percentage of Si precipitated is large relative to the solution [Si]. This means that the dissolution rate  $r_+$  can be measured while Si precipitation occurs (Zhu et al., 2016).

With  $r_+$  fixed by the Si isotope ratios,  $r'_{\text{pre, Si}}$  can be derived from the mass balance for [Si] in Eq. (5); in practice,  $f_{28,\text{t}}$  and  $f_{29}$  are not independent in the experiments because  $^{30}\text{Si}/^{28}\text{Si}$  are fixed. Similarly, the mass transfer rate of Al (from solutions to solids) can be calculated from a mass balance equation for Al similar to that for Si in Eq. (5).

The mass balance alone cannot distinguish between the reverse reaction (feldspar precipitation) and secondary phase precipitation. Consequently,  $r'_{pre,Si}$  and  $r'_{pre,Al}$  stand for the rates of removal of Si and Al from solution (mol  $L^{-1}$  s<sup>-1</sup>) as combined results of all precipitation reactions that occur in the system. These rates (and the mass) can be, however, precisely known.

The isotope tracer experiments provide a different kind of rate data—unidirectional dissolution rates,  $r_+$ , independent of  $\Delta_r G$ . With  $r_+$  available, it becomes clear that the reduced  $r_{\rm net}$  from the  $f(\Delta_r G)$  relationship implies the precipitation of feldspars at the near-equilibrium conditions. It is discussed below that these unidirectional rates can be used in models of weathering systems in which the reverse reactions of precipitation are negligible for feldspars.

#### 3. MATERIALS AND METHODS

#### 3.1. Feldspar grains preparation

Research grade albite crystals (from Amelia Court House, Virginia, USA) were purchased from Ward's Natural Sciences Establishment, Inc. The crystals were handpicked, ground with a clean tungsten carbide mortar and pestle, and subsequently dry-sieved through a clean copper mesh to retain the 53– $106\,\mu m$  fraction. For the freshly ground materials, there were many submicron-to-micron particles that adhered to the surface of large grains. The dissolution of these ultra-fine particles may result in initially nonlinear rates of reaction or parabolic kinetics (Holdren and Berner, 1979; Lu et al., 2013). To remove these particles, the ground feldspar sample was ultrasonically rinsed with ethanol eight times for about 20 minutes per treatment. The cleaned albite grains were then air-dried overnight and subsequently saved in a desiccator.

Pink perthitic specimen (from Madawaska, Ontario, Canada) was also purchased from Ward's Natural Sciences Establishments, Inc. The crystals were handpicked, ground with a clean tungsten carbide mortar and pestle, and subsequently dry-sieved through a clean copper mesh to retain the 53–106 μm fraction. Similarly, the freshly ground powders were first ultrasonically rinsed with ethanol eight times for 20 minutes per treatment to remove submicron-tomicron sized particles. Then the powders were exchanged in molten KCl (K-feldspar: KCl = 1:30, weight ratio) at 900 °C for 48 h in Pt crucibles in a muffle furnace to prepare a sodium-free K-feldspar (pure microcline). After the exchange reaction, these samples were again ultrasonicated and rinsed with ethanol three times for 10 minutes per treatment. The samples were stored in a desiccator.

#### 3.2. Mineral characterization

The purity of the albite and treated perthite were examined with powder X-ray diffraction (XRD), using a Bruker D8 Advance diffractometer, equipped with a Cu anode at 20 kV and 5 mA, and with a SolX energy-dispersive detector. The scan parameters used were 2–70°2θ, with a step size of 0.02°2θ. Starting samples were ground by hand in an agate mortar and pestle to get sufficient small particles. These particles were subsequently filled into a titanium sample holder for XRD analysis. The albite sample was made up of 95.05% low albite, 2.94% muscovite, and 2.01% quartz. The mineral composition of annealed, sodium-free K-feldspar, was 90.74% maximum microcline, 0.58% albite, 1.69% quartz, and 6.99% muscovite.

A Beckman Coulter SA-3100 surface area analyzer was used for the BET (Braunauer et al., 1938) surface area analysis of albite and K-feldspar grains before the experiments. The samples were degassed at 250 °C overnight prior to measurements. The instrument was calibrated before and periodically during measurements, using the National Institute of Standards and Technology reference material 1900, a silicon nitride powder with a surface area of 2.85 m²/g. Multipoint  $N_2$  gas adsorption isotherms were measured to obtain BET-specific surface area of samples (Lu et al., 2013). The specific surface area of albite was 0.143 m²/g and the surface area of annealed K-feldspar was 0.201 m²/g, with an analytical error within  $\pm$  10%.

Scanning Electron Microscopy (SEM) was conducted with a Quanta 400 Field Emission Gun (FEG). The Energy Dispersive X-ray Spectrometer (EDS) system has an EDAX thin window and CDU LEAP detector. The low energy X-ray detection with FEG provided high spatial resolution

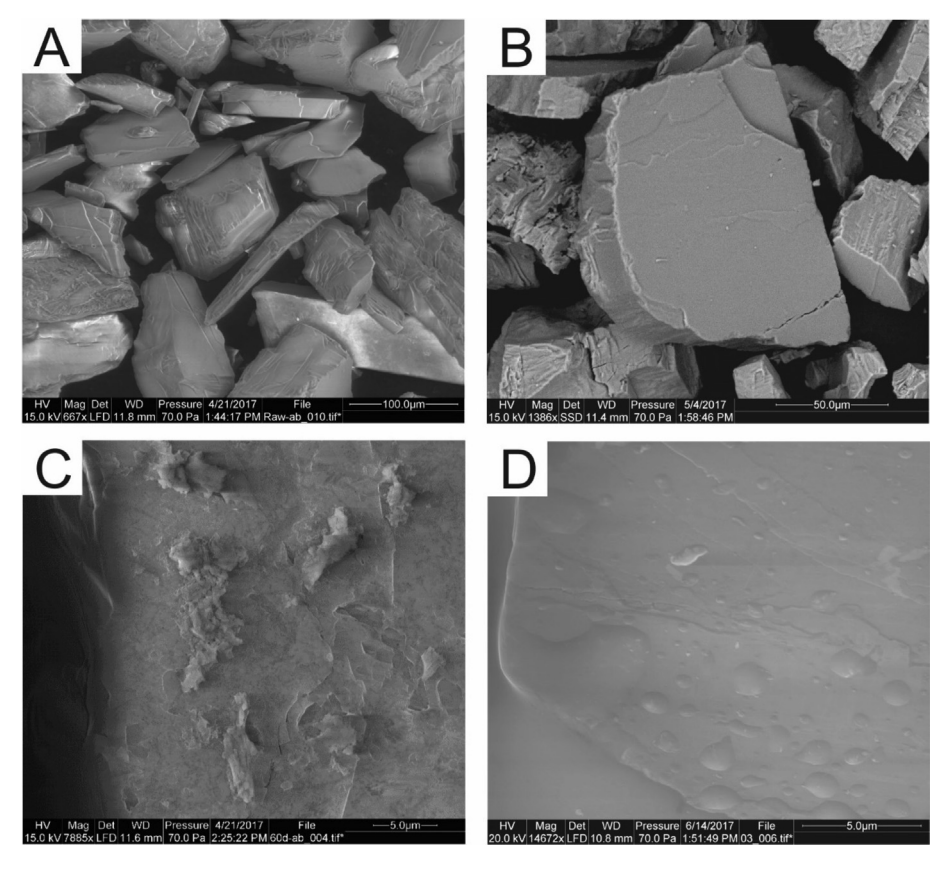


Fig. 3. Field emission gun-SEM micrographs: (A) unreacted albite grains; (B) unreacted, KCl-exchanged microcline grains; (C) albite after 1440 h of reaction (N-4); and (D) K-feldspar grains after 720 h of reaction (K-5). Amorphous precipitates were present on both albite and K-feldspar surfaces.

for microanalysis down to  $\sim$ 0.1  $\mu$ m<sup>2</sup> under optimum conditions. SEM images are shown in Fig. 3.

## 3.3. <sup>29</sup>Si stock solution for isotope tracer experiments

Except where noted, all chemicals used were analytical grade. In order to prepare the <sup>29</sup>Si stock solution, <sup>29</sup>SiO<sub>2</sub> enriched powder (with isotope abundance of 0.0004 <sup>28</sup>Si, 0.9990 <sup>29</sup>Si, and 0.0006 <sup>30</sup>Si from Isoflex, San Francisco, CA, USA) were dissolved by alkali flux (Georg et al., 2006). Briefly, 0.0488 ( $\pm 0.001$ ) g of <sup>29</sup>SiO<sub>2</sub> powder and 0.4880 (±0.001) g of NaOH were placed in a silver crucible that was subsequently put into a 730 °C preheated muffle furnace and held for 10 minutes. After cooling to room temperature, the mixture was dissolved in 500 ml DI water (18.2 M $\Omega$ , Millipore) and the solution was then transferred into a clean 500-ml polypropylene bottle. Then, the solution (i.e., 1.6 mM <sup>29</sup>SiO<sub>2</sub>) was poured into a vacuum filter system (Thermo Scientific, Nalgene, sterile analytical filter) which used a piece of 0.22-µm nitrocellulose membrane filter paper (Fisher Scientific, Pittsburgh, PA, USA). The filtered stock solution was collected into a new, clean 500-ml polypropylene bottle and stored in a refrigerator at 4.0 °C.

#### 3.4. Dissolution experiments with isotope tracer

The initial solution was prepared by dissolving a certain amount of KNO3, Al(NO3)3.9H2O and NaNO3 into DI water in each wide-mouth polypropylene bottle, and adding <sup>29</sup>SiO<sub>2</sub> stock solution, with a final solution volume of  $\sim$ 250 mL. The amounts of KNO<sub>3</sub>, NaNO<sub>3</sub>, Al(NO<sub>3</sub>)<sub>3</sub>·9H<sub>2</sub>O, <sup>29</sup>SiO<sub>2</sub> stock solution, and DI water were recorded. The concentrations of each constituent in each experiment are listed in Table 2. The pH of the initial solution was thereafter measured and adjusted by adding a small amount of HNO<sub>3</sub> or NaOH at 50 °C to pH  $\sim$  6-7. The solution was subsequently filtered with 0.22-µm nitrocellulose membrane filter paper to remove possible precipitates. Additionally, 1.000 ( $\pm 0.001$ ) g of albite and purified K-feldspar and 10 g (i.e., ~10 mL) initial solution with different pH were mixed in a 30-mL polypropylene bottle to initiate mineral dissolution. Overall, several polypropylene bottles were prepared for each group of batch experiments. The polypropylene bottles were sealed with plastic wrap and heated to  $50 \pm 0.5$  °C in a water bath (VWR General Purpose Water Bath) for the duration of the experiment.

table 2 Chemistry of experimental solutions at 15 min after initiating the reactions

Exp#	pH @50 °C	[Si] µmol/kg	[Na] µmol/kg	[K] µmol/kg	[Al] µmol/kg	SI (kf)	SI (ab)	SI (kln)	SI (qtz)	$SI (allo)^a$	SI (imo) <sup>b</sup>
4-N	5.94	279	909	N/A	1.14	N/A	-1.43	6.72	-0.1	4.14	4.78
Z-S	6.14	278	644	N/A	0.67	N/A	-1.57	6.01	-0.1	3.43	4.07
K-5	6.05	98	52	878	0.35	-2.88	-4.52	4.54	-0.62	2.41	3.16
K-7	6.77	19	73	475	1.37	-4.43	-5.64	3.19	-1.28	1.58	2.48
K-9	7.77	16	61	926	105	-2.5	-4.08	4.82	-1.37	3.28	4.19

<sup>a</sup> The SI value is for allophane with Al/Si of 1.64, see Su and Harsh (1998) for details. <sup>b</sup> The SI value is for synthetic imogolite, see Su and Harsh (1994) for details.

#### 3.5. Sampling of dissolution experiments

At pre-determined sampling intervals, the solution was poured into a vacuum filter system (Thermo Scientific, Nalgene, sterile analytical filter) that used a piece of 0.22 µm nitrocellulose membrane filter paper (Fisher Scientific, Pittsburgh, PA, USA) to filter the solution. The filtered solution was divided into three equal fractions ( $\sim$ 3 ml each) for Si isotope analysis, Si concentration determination, and cation analysis. The pH of the solution was measured at room temperature—22.5 (±0.5) °C—with the Si concentration fraction determined immediately after sample collection using an Orion<sup>TM</sup> 8102BNUWP ROSS Ultra<sup>TM</sup> pH Electrode. The reported accuracy was  $\pm 0.02$  pH units (i.e.  $\pm 4.5\%$  in H<sup>+</sup> activity). In order to make the solution unsaturated with respect to its secondary phases (e.g., kaolinite, gibbsite, imogolite, allophane, amorphous SiO2 and Al (OH)<sub>3</sub>), the solution for cation analysis was acidified with 1-2 drops of 12 N HCl solution.

### 3.6. Sample pre-treatment before isotopic analysis

To reduce the disturbance from other cations when measuring silicon isotope, all solution samples were purified by cation exchange chromatography. Details about the chemical procedure are described in Georg et al. (2006). Briefly, 1.8 mL Bio-Rad AG 50 W-X8 resin was placed in a 10-mL Poly-Prep chromatography column. The resin was rinsed with hydrochloric acid and DI water as follows: 6.0 mL DI water, 6.0 mL 3.0 N HCl, 6.0 mL 6.0 N HCl, 4.0 mL 37% HCl, 6.0 mL 6.0 N HCl, 10 mL 3.0 N HCl, and thrice 5.0 ml DI water. Then 1.0 mL solution sample was added to the column to condition the resin. Afterward, 7.0 ml of the solution sample was loaded onto the column and the filtered solution was collected in a clean polystyrene 15-ml conical centrifuge tube (Fisher Scientific, Pittsburgh, PA, USA) in preparation for isotope analysis.

#### 3.7. Measurements of silicon stable isotopes

The Si isotope ratios were measured using highresolution multiple-collector inductively coupled plasma mass spectrometry (HR-MC-ICP-MS, Nu Plasma II, Wrexham, UK) at Northwest University, China. Blank samples were filled with ultrapure DI water and acidified with ultrapure HNO<sub>3</sub>. The Si isotope ratios were measured using Faraday cups under static mode. Instrumental sensitivity was  $\sim \! 11 \ V \ \mu g^{-1} \ g^{-1}$  for  $^{28}Si$  in high-resolution mode. The fractions of  $^{28}Si$ ,  $^{29}Si$ , and  $^{30}Si$  were calculated by the measured <sup>28</sup>Si/<sup>29</sup>Si and <sup>28</sup>Si/<sup>30</sup>Si ratios. The sample solution was introduced into MC-ICP-MS using a dry aerosol system (Aridus II, Cetac, USA) and a 100 µL min<sup>-1</sup> PFA micro-flow nebulizer. Sample standard bracketing (SSB, Alfa Aesar Si, Stock# 38717, LOT 591543G) was adopted to calibrate the instrument isotopic bias. The isotopic abundance of every sample was determined by averaging the three duplicate measurements using the Time-Resolved-Analysis (TRA) method. The relative standard deviation (RSD) of the three ratios was used to evaluate the data quality. Only those analyses with RSD ( $\delta^{30}$ Si) < 10% were reported; samples with RSD  $(\delta^{30}Si) > 10$  % were remeasured.

#### 3.8. Determination of Si and cation concentrations

Total dissolved Si concentrations (i.e., [Si]) were analyzed with Perkin Elmer Lambda 2S UV–visible spectrophotometer, using the molybdate blue method (Govett, 1961). The uncertainty in measured Si was less than  $\pm 5\%$  for concentrations above 4  $\mu$ M. Detection limits for analyses of Si were less than 0.05 ppm (or 2  $\mu$ M). Total cation concentrations of Na<sup>+</sup>, Al<sup>3+</sup>, and K<sup>+</sup> were analyzed with inductively coupled plasma–quadrupole mass spectrometry (ICP-QMS) Agilent 7700x with a measurement uncertainty of  $\pm 5\%$ . The detection limit for analyses of Al was about 10 ppb.

#### 3.9. Calculations of mineral saturation indices (SI)

Based on the measured concentrations of Si, Al, Na and K, and pH, SI for albite and K-feldspar were calculated with the aid of the software PHREEQC 3.5.0 (Parkhurst and Appelo, 2013). In situ pH was calculated following the method of Zhu and Lu (2009). An internally consistent dataset of equilibrium constants for relevant mineral and aqueous species at 50 °C was constructed using SUPCRTBL (Zimmer et al., 2016). Equilibrium constants (log K) for selected reactions are shown in Table 3. The thermodynamic properties of K-feldspar differ significantly due to compositional and structural variations (Arnórsson and Stefánsson, 1999). Using the value of  $\Delta_f G^o$  for K-feldspar from Holland and Powell (2011) would result in an SI of  $\sim$ +2.0. We

followed the practice of Gautier et al. (1994) and Alekseyev et al. (2004), and calculated an effective Q/K from the solution composition of long-term experiments and set the SI = 0 for analysis. The re-setting of SI of 0 for K-feldspar does not suggest true equilibrium with K-feldspar in our experiments; it is for the convenience of discussing dissolution at the steady-state, presumably near-equilibrium with respect to K-feldspar. For amorphous  $SiO_2$  and  $Al(OH)_3$ , the log Ks were taken from Stefansson (2001). For allophane and imogolite, the thermodynamic properties were calculated based on the experimental data in Su and Harsh (1994; 1998). The Gibbs free energy at standard state for those species was adjusted to ensure the internal consistency with other species.

#### 4. RESULTS

# 4.1. SEM, XRD, and Transmission Electron Microscope (TEM) examination of solid reactants and products

SEM micrographs of albite were taken from the series before reaction (Fig. 3A) and after 1440 h of reaction (Fig. 3C). A small amount of secondary precipitation was observed on samples after 1440 h of reaction. SEM images of annealed K-feldspar before and after 720 h of reaction are shown in Fig. 3B and D, respectively. After interacting with an aqueous solution for 720 h, the surface of the annealed K-feldspar was covered with amorphous precipitates.

Multiple attempts were made to collect small particles of secondary phases following specialized procedures to identify the secondary phases with XRD (Huifang Xu, personal

Table 3				
Equilibrium	constants	of relevant	chemical	reactions.

Species	Reaction	Log K at 50 °C
Aqueous Species		
OH-	$H_2O = OH^- + H^+$	-13.271
$Al(OH)^{2+}$	$H_2O + AI^{3+} = AI(OH)^{2+} + H^+$	-4.222
$Al(OH)_2^+$	$2H_2O + AI^{3+} = AI(OH)_2^+ + 2H^+$	-9.379
Al(OH) <sup>o</sup> <sub>3</sub>	$3H_2O + AI^{3+} = AI(OH)_3^0 + 3H^+$	-14.964
$Al(OH)_4^-$	$4H_2O + AI^{3+} = AI(OH)_4^- + 4H^+$	-20.435
NaAl(OH) <sup>o</sup> <sub>4</sub>	$4H_2O + Na^+ + Al^{3+} = NaAl(OH)_4^0 + 4H^+$	-20.310
AlH <sub>3</sub> SiO <sub>4</sub> <sup>2+</sup>	$A1^{3+} + SiO_2^0 + 2H_2O = AlH_3SiO_4^{2+} + H^+$	-1.597
NaOH°	$Na^+ + H_2O = NaOH^o + H^+$	-13.464
HSiO <sub>3</sub>	$SiO_2^o + H_2O = HSiO_3^- + H^+$	-9.483
NaHSiO <sub>3</sub> <sup>o</sup>	$SiO_2^o + H_2O + Na^+ = NaHSiO_3^o + H^+$	-7.923
Mineral Phase		
Albite	$Al^{3+} + Na^{+} + 2H_2O + 3SiO_2^o = Albite + 4H^{+}$	-1.735
Microcline	$A1^{3+} + K^{+} + 2H_{2}O + 3SiO_{2}^{o} = Microcline + 4H^{+}$	-0.188
Kaolinite	$2AI^{3+} + 5H_2O + 2SiO_2^o = Kaolinite + 6H^+$	0.626
Quartz	$SiO_2^o = Quartz$	3.445
Gibbsite	$Al^{3+} + 3H_2O = Gibbsite + 3H^+$	-6.334
SiO <sub>2</sub> (am)	$SiO_2^o = SiO_2(am)$	2.535
Al(OH) <sub>3</sub> (am)	$Al^{3+} + 3H_2O = Al(OH)_3(am) + 3H^+$	-8.339
Imogolite	$2A1^{3+} + 5H_2O + SiO_2^o = Imogolite + 6H^+$	-8.329
Allophane(1.26)	$2A1^{3+} + 5.63H_2O + 1.59SiO_2^o = Allophane(1.26) + 6H^+$	-6.677
Allophane(1.64)	$2A1^{3+} + 5.5H_2O + 1.22SiO_2^o = Allophane(1.64) + 6H^+$	-8.187
Allophane(2.02)	$2A1^{3+} + 5.53H_2O + 1SiO_2^o = Allophane(2.02) + 6H^+$	-9.387
Analcime	$Al^{3+} + Na^{+} + 3H_2O + 2SiO_2^{0} = Analcime + 4H^{+}$	-5.950

10)<sup>b</sup>

communication). However, XRD patterns showed only feldspar peaks. Attempts were also made to identify the secondary phases with TEM (Hiromi Konishi, Personal communication). The results were not conclusive.

However, the amounts of Si and Al precipitated were quantified in these isotope tracer experiments (see below). For example, the total precipitated Si in Experiment N-4 was  $\sim\!5~\mu mol$  from Day 15 to Day 60. If we assume that the precipitated Si all went into amorphous kaolinite, the precipitated secondary phase is only 0.06 wt% of the solids in the reactors. Such small amounts could not be detected with XRD, but are significant to rate calculations. Apparently, isotope ratios are more sensitive detectors of secondary phase precipitation in near-equilibrium experiments than XRD and SEM.

#### 4.2. Si isotopes and solution composition

All analyses below refer to the steady-state phase of the experiments. These are Day 15–60 for albite experiments and Day 10–30 for K-feldspar experiments. The "hiatus" of the initial phase of the experiments was not used in rate analysis.

The chemical compositions of the experimental solutions are shown in Table 4. The temporal evolution of Si isotope fractional abundances is shown in Fig. 4. During the entire period of these experiments, the  $^{28}$ Si fraction of the solution ( $f_{28}$ ) increased and the  $^{29}$ Si fraction ( $f_{29}$ ) decreased monotonically. Si concentration data are shown in Fig. 5 and all show a monotonic increase over time. The albite and K-feldspar experiments are in the pH range of 6.34–7.56 (neutral pH at 50 °C is 6.64). All data are provided in the Electronic Annex as well as at Indiana University's institutional data repository IUSchorlarWorks at https://doi.org/10.5967/v1mc-0736.

Calculated SI for albite were at constant values of near-zero after 240 h of reaction and for K-feldspar a near-constant value of +1.94 after 360 h, which was operationally re-set to zero in Section 3.9 (Figs. 6 and 7). At SI of near-zero (see the assumptions in Section 3.9), feldspar dissolution continued throughout the experiment (albite for 1440 h and K-feldspar for 720 h). Si concentrations increased except for K-7. Al concentration decreased. The Na and K concentrations increased (Fig. 8).

The aqueous solutions in both albite and K-feldspar experiments were supersaturated with respect to gibbsite, amorphous Al(OH)<sub>3</sub>, kaolinite, allophane, and imogolite (Figs. 6 and 7). The two albite experimental solutions have SI near-zero for quartz. The SI values for the secondary minerals were also constant, starting at 360 h and remaining constant for 720 h of K-feldspar reaction and 1440 h of albite. On activity-activity diagrams (not shown), all data points fell within the kaolinite stability field. Notably, the albite experimental solutions fell on the lines at equilibrium with quartz and amorphous Al(OH)<sub>3</sub>. All experimental solutions were undersaturated with respect to amorphous silica (Fig. 9).

Eq. (7) was used to find the steady-state feldspar dissolution and Si precipitation rates from the Si isotope ( $f_{28}$  and  $f_{29}$ ) (Fig. 4). The best-fitted values, calculated with a

Chemical composition of experimental solutions at the end of reaction.8

	o monitodinos	experimental solution	chemical composition of orporations at the original control of the original co	cuom:							
Exp#	pH 50 °C	[Si] µmol/kg	[Na] µmol/kg	[K] µmol/kg	[Al] µmol/kg	SI(kfs)	SI(ab)	SI(kln)	SI(qtz)	$SI (allo)^a$	SI (imc
7-Y	6.34	375	694	N/A	7	N/A	-0.08	8	0.03	5.21	5.82
N-5	6.43	396	787	N/A	7	N/A	-0.05	7.9	0.05	5.12	5.73
K-5	7.17	188	626	797	16	-0.00	-1.4	6.71	-0.1	4.31	5.00
K-7	7.31	148	505	478	27	-0.16	-1.36	6.55	-0.22	4.24	4.94
K-9	7.56	100	720	1440	<i>L</i> 9	-0.42	-2.05	6.21	-0.4	4.05	4.78
1			ŧ								

<sup>&</sup>lt;sup>a</sup> The SI value is for allophane with Al/Si of 1.64, see Su and Harsh (1998) for details. <sup>b</sup> The SI value is for synthetic imogolite, see Su and Harsh (1994) for details.

1440 hours for albite, 720 hours for K-feldspar

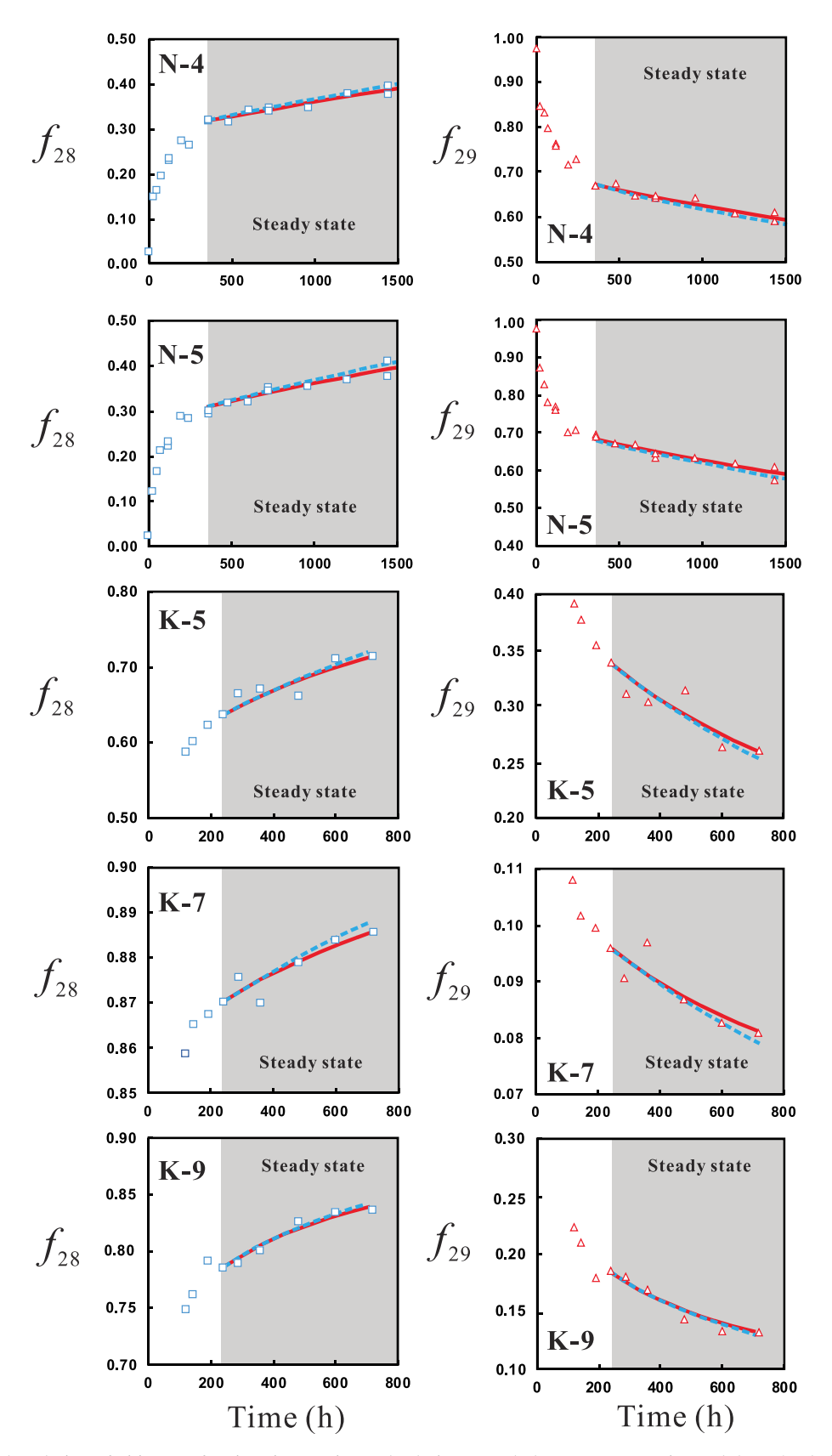


Fig. 4. Temporal evolution of Si isotope fractions in experimental solutions. Symbols represent experimental data. Analytical uncertainties for isotope fraction ( $f_{28}$  and  $f_{29}$ ) are less than  $\pm 0.001(2\sigma)$ , which is smaller than the symbols. Red and blue lines are calculated from Eq. (7) assuming without and with Si precipitation, respectively. The shaded area identifies conditions where the feldspar saturation indices remained constant over time (i.e. a steady-state condition).

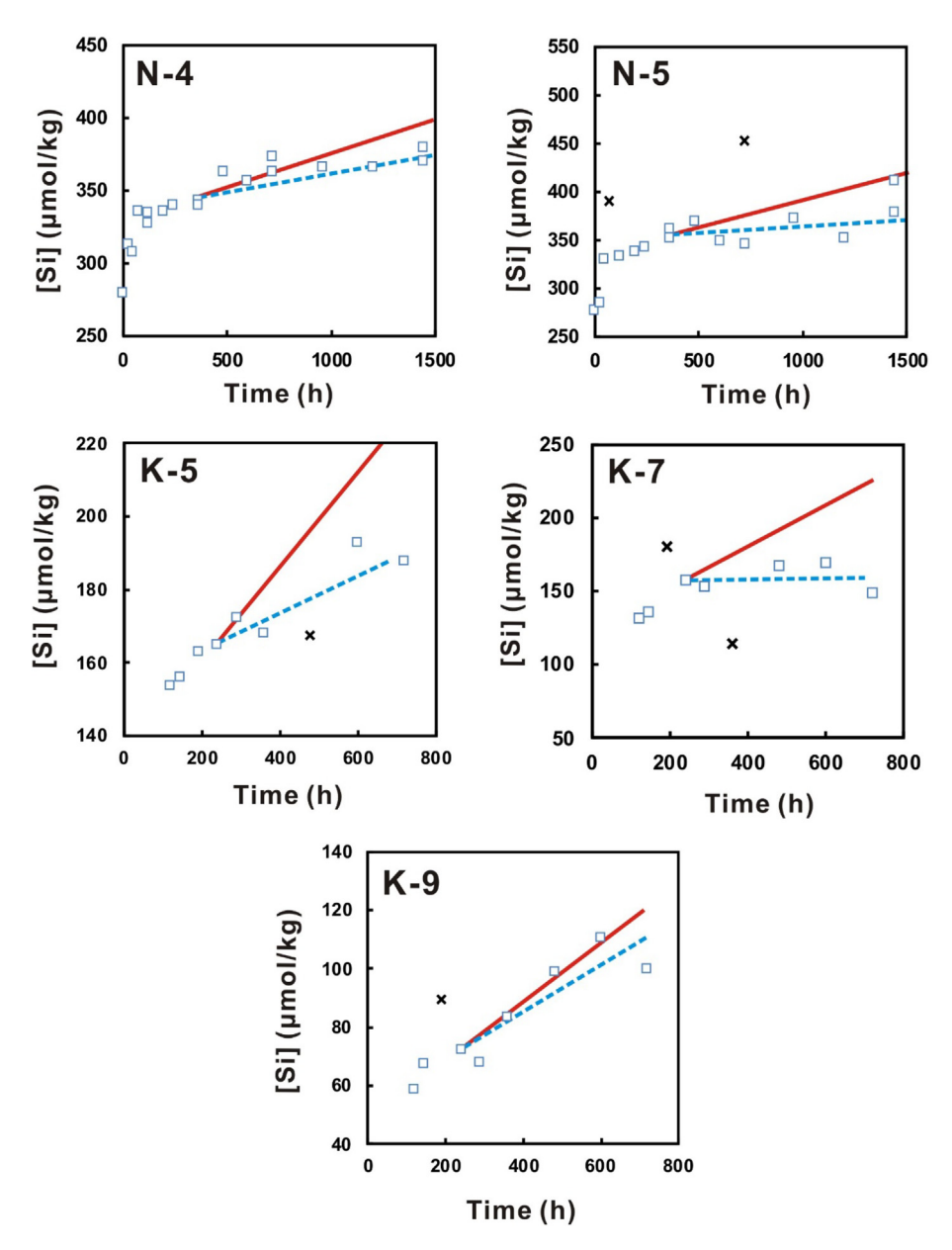


Fig. 5. Temporal evolution of Si concentrations. Symbols represent experimental data. [Si] analytical uncertainties are about  $\pm 5\%$ . Red solid lines are Si concentrations predicted from feldspar dissolution rates fitted in Fig. 4 assuming no Si precipitation and using Eq. (5) with  $r'_{\text{pre}, Si} = 0$ . Blue dotted lines represent the best fit of  $r'_{\text{pre}, Si}$  that considers Si precipitation using Eq. (5). The difference between the two lines gives the Si precipitation flux. Data points marked with a black x were not included in rate calculations. (For interpretation of the references to colour in this figure legend, the reader is referred to the web version of this article.)

solver in Excel<sup>®</sup>, are given in Tables 5a and 5b. Si and Al precipitation rates were calculated from the differences between predicted Si concentrations based on the dissolution rates (fixed by isotope ratios) and the experimentally observed Si and Al concentrations (Fig. 5). Because the initial solution was ~100% <sup>29</sup>Si and dissolution of feldspar only adds <sup>29</sup>Si into the solutions, [<sup>29</sup>Si] should increase over time; a decrease in [<sup>29</sup>Si] indicates Si precipitation, which was observed in these experiments. As demonstrated in Zhu et al. (2016), Si precipitation reduces the total Si concentration but does not noticeably change Si isotope ratios. This allows unidirectional dissolution rates to be measured

even when Si is precipitating. This is demonstrated again in Fig. 4, which shows that the predicted isotope fraction evolution curves calculated with dissolution only coincide with those calculated with dissolution plus Si precipitation.

### 5. DISCUSSION

# 5.1. Contextualizing rates from isotope tracer experiments

The rates obtained in this study are unidirectional dissolution rates,  $r_{+}$ , and not net rates,  $r_{\text{net}}$ . This sets them apart from previously measured near-equilibrium rates in the

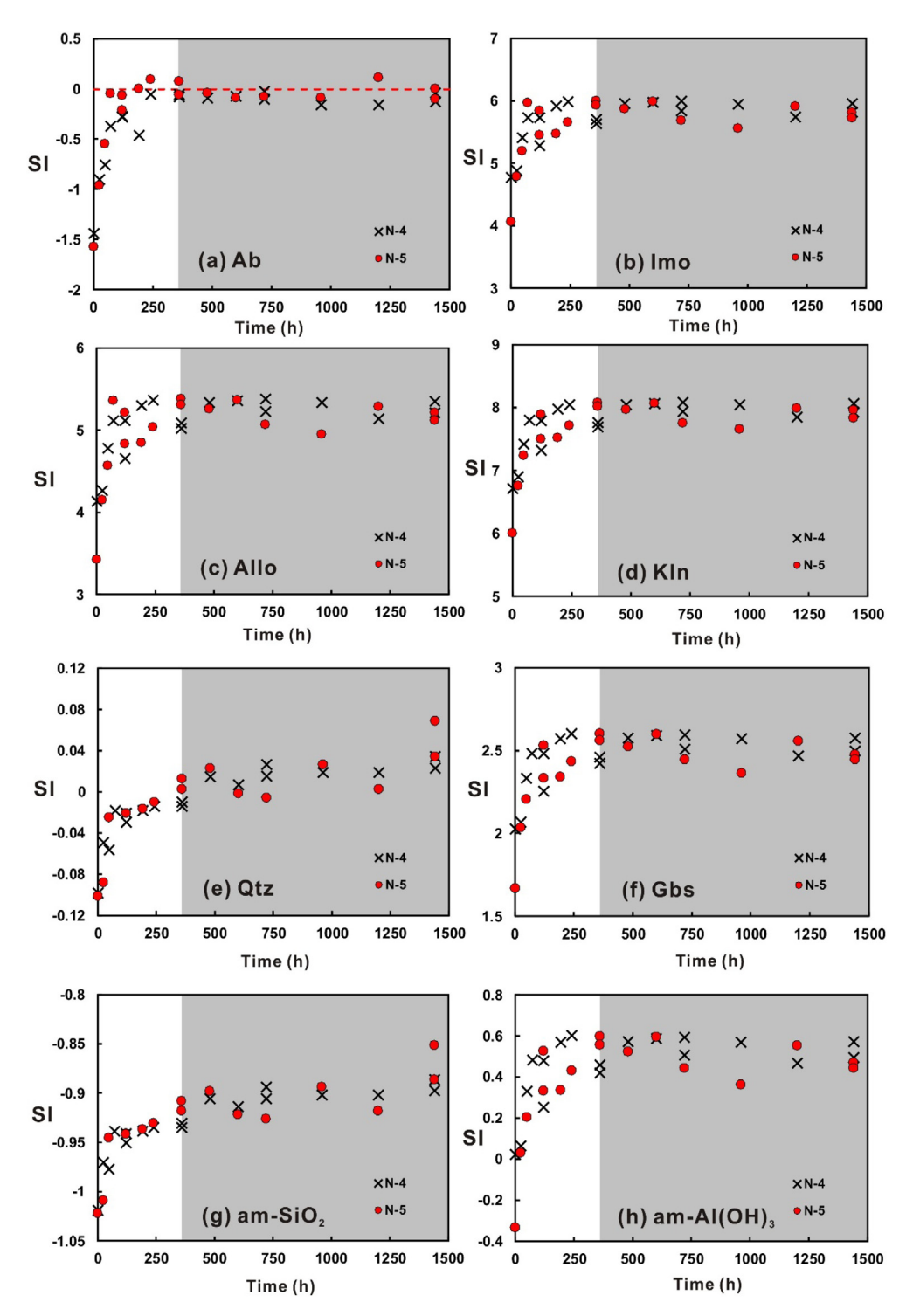


Fig. 6. Temporal evolution of saturation indices (SI =  $\log (Q/K)$ ) of (a) albite, (b) imogolite, (c) allophane, (d) kaolinite, (e) quartz, (f) gibbsite, (g) amorphous SiO<sub>2</sub>, and (h) amorphous Al(OH)<sub>3</sub> during albite dissolution experiments. The SI of the solutions was nearly constant after 15 days (grey region).

literature, which are all net rates. A significant amount of Si precipitated in our near-neutral pH experiments as the experimental solutions were supersaturated with respect to many secondary phases. However, the experimental results demonstrate that the isotope tracer method worked

well, as the precipitation of Si-bearing phases changed little of the Si isotope ratios (Fig. 4). Under this circumstance, the conventional method that relies on [Si] would have failed. For example, if the [Si] were used to retrieve the albite dissolution rate for Experiment N-4, an artifact of

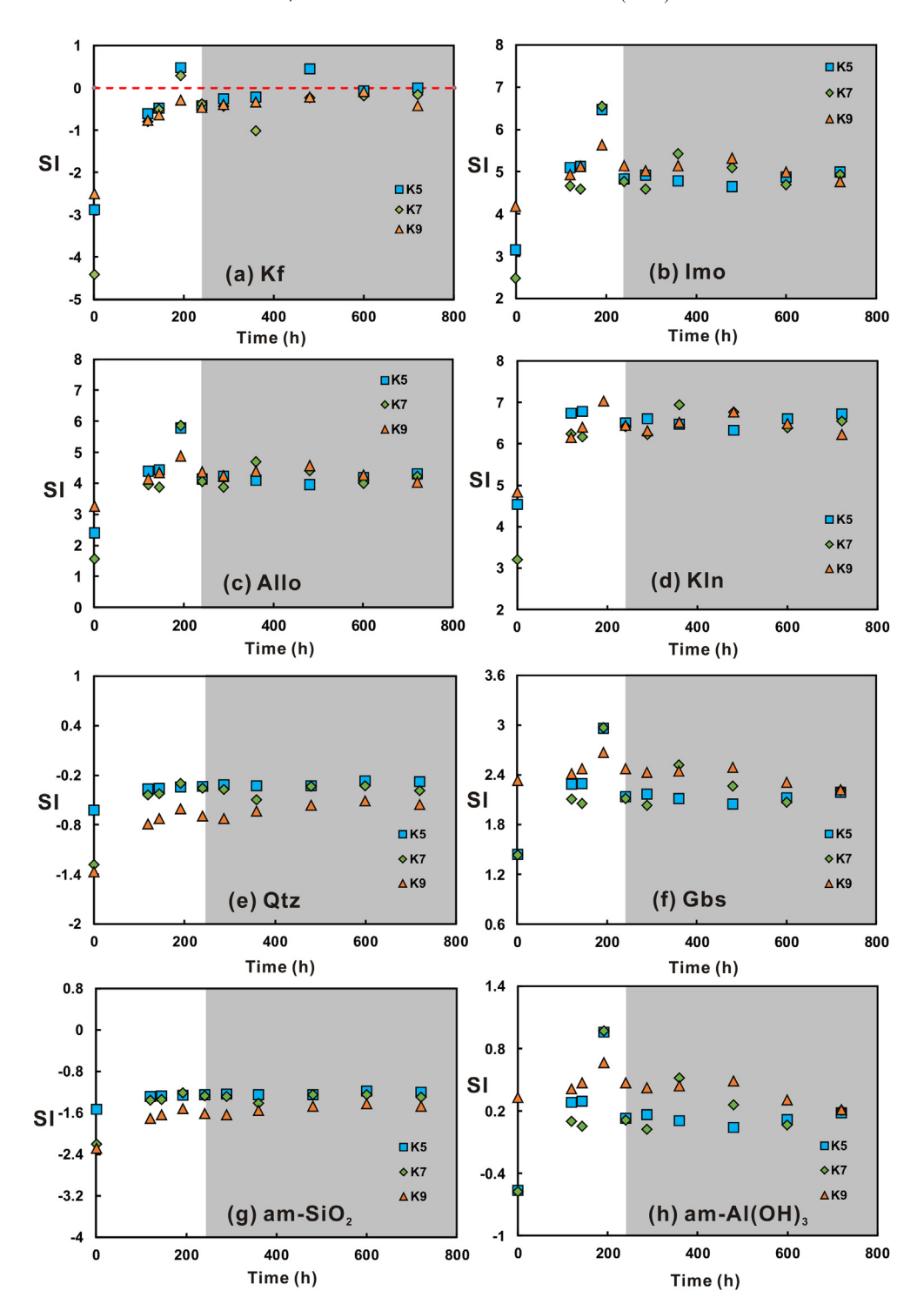


Fig. 7. Temporal evolution of saturation indices ( $SI = \log(Q/K)$ ) of (a) K-feldspar, (b) imogolite, (c) allophane, (d) kaolinite, (e) quartz, (f) gibbsite, (g) amorphous SiO<sub>2</sub>, and (h) amorphous Al(OH)<sub>3</sub> during the K-feldspar dissolution experiments. The SI of solutions was nearly constant after 10 days (grey region).

a factor of 1/3 less would be introduced because of Si precipitation. Fig. 10 compares the unidirectional dissolution rate,  $r_+$ , with the apparent net rates,  $\tilde{r}_{net}$ . Note that the "true" dissolution rates were consistent while the apparent dissolution rates varied from experiment to experiment

because the precipitation of the secondary phase was more random.

There is a relatively large amount of experimental data on feldspar dissolution kinetics in the literature and they have been reviewed extensively (Blum and Stillings, 1995;

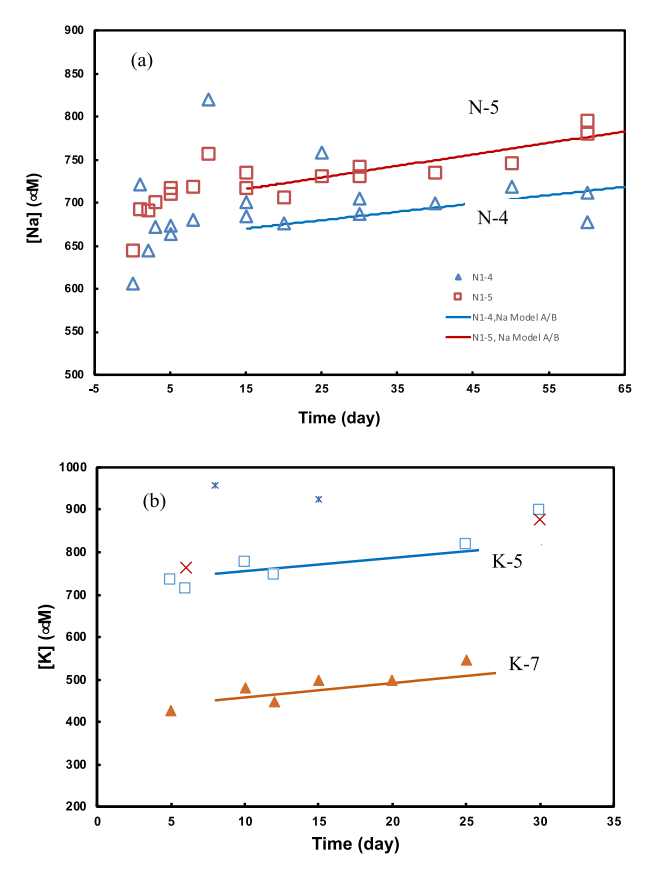


Fig. 8. Temporal evolution of Na<sup>+</sup> (a) and K<sup>+</sup> (b) concentrations. Symbols represent experimental data. Lines are concentrations predicted from rates fitted in Fig. 4 using Si isotope ratios; they are not fitted to the experimental data. The outliers of [K<sup>+</sup>] data are represented with different symbols but the same color. Data from experiment K-9 show no trends.

Palandri and Kharaka, 2004; Marini, 2007; Brantley, 2008; Marty et al., 2015). The unidirectional dissolution rates from this study would be comparable to the far-fromequilibrium dissolution rates in the literature if reaction mechanisms do not change from far-from-equilibrium to near-equilibrium. At 50 °C, there are no experimental data available for albite at near-neutral pH (Palandri and Kharaka, 2004). Our  $r_+$  values are 1.5 log units lower than the values calculated from the rate equation recommended by Palandri and Kharaka (2004). Chou and Wollast (1984) measured at 25 °C albite dissolution rates far-fromequilibrium at pH < 6 and >8. Palandri and Kharaka (2004) used their experimental data to regress the pH dependence. With the necessary temperature and pH extrapolation using the parameters recommended by Palandri and Kharaka (2004), our  $r_{+}$  values are also 1.5 log units lower than those of Chou and Wollast (1984). For K-feldspar, much less experimental data are available in the literature and the quality of data is of concern. There are no experimental data available near-neutral pH at 50 °C or lower temperature. Our  $r_+$  values are 0.5 log units lower than the value calculated from the rate equation recommended by Palandri and Kharaka (2004).

There are insufficient experimental data to explain why the  $r_+$  values obtained from near-equilibrium conditions in this study are slower than  $r_+$  values at far-from-equilibrium conditions in the literature. However, this difference may result from a switch of feldspar dissolution from a non-etch pit to an etch pit controlled mechanism at a critical departure from equilibrium (Lasaga and Blum, 1986; Burch et al., 1993; Dove et al., 2005; Lüttge, 2006; Brantley, 2008; Arvidson and Luttge, 2010; Gruber et al., 2014). A second explanation could be, within TST, a control of dissolution by an Al-free precursor complex

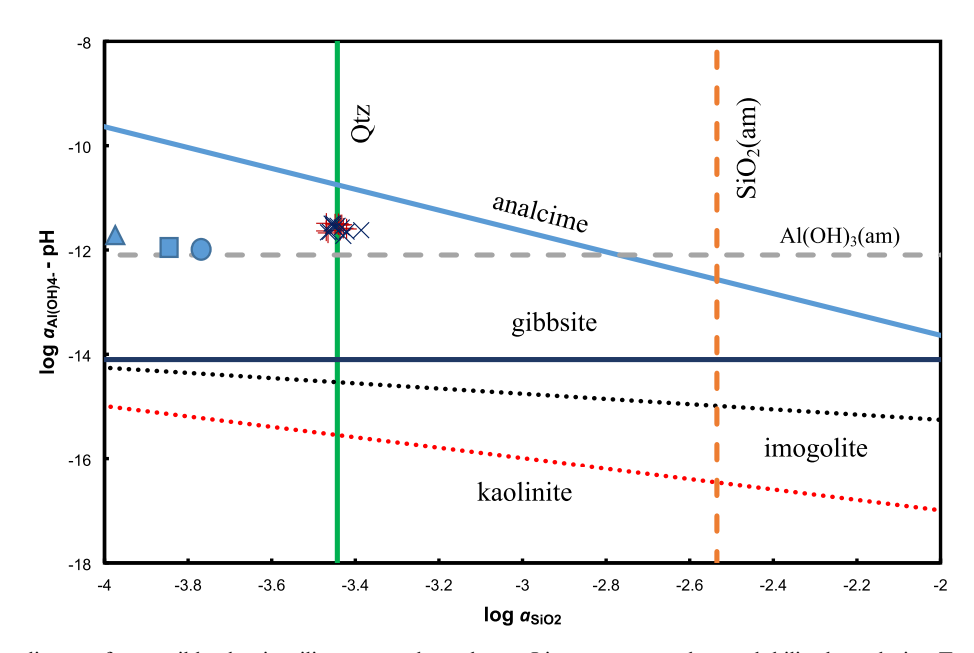


Fig. 9. Solubility diagram for possible aluminosilicate secondary phases. Lines represent phase solubility boundaries. To plot the solubility boundary of Na-bearing analcime, the average Na concentration (710.6  $\mu$ mol/L) in N-4 and N-5 experiment samples was used. Crosses and Xs denote albite experiments; solids symbol K-feldspar experiments.

Table 5a Calculated rates for albite experiments.

	N-4	N-5
Albite forward reaction rate, $r_+$ (mol albite m <sup>-2</sup> s <sup>-1</sup> )	$2.62 \times 10^{-13}$	$3.17 \times 10^{-13}$
Albite forward reaction rate, $r'_{+}$ (mol Si L <sup>-1</sup> s <sup>-1</sup> )	$1.13 \times 10^{-11}$	$1.53 \times 10^{-11}$
Si precipitation rate, $r'_{\text{pre,Si}}$ (mol Si L <sup>-1</sup> s <sup>-1</sup> )	$9.14 \times 10^{-12}$	$9.79 \times 10^{-12}$
Al precipitation rate, $r'_{\text{pre,Al}}$	$4.27 \times 10^{-12}$	$5.26 \times 10^{-12}$

Table 5b Calculated rates for K-feldspar experiments.

	K-5	K-7	K-9
Kfs forward reaction rate, $r_+$ (mol feldspar m <sup>-2</sup> s <sup>-1</sup> )	$5.97 \times 10^{-13}$	$6.52 \times 10^{-13}$	$4.67 \times 10^{-13}$
Kfs forward reaction rate, $r'_+$ (mol Si L <sup>-1</sup> s <sup>-1</sup> )	$3.60 \times 10^{-11}$	$3.91 \times 10^{-11}$	$2.81 \times 10^{-11}$
Si precipitation rate, $r'_{\text{pre,Si}}$ (mol Si L <sup>-1</sup> s <sup>-1</sup> )	$2.18 \times 10^{-11}$	$3.80 \times 10^{-11}$	$5.95 \times 10^{-12}$

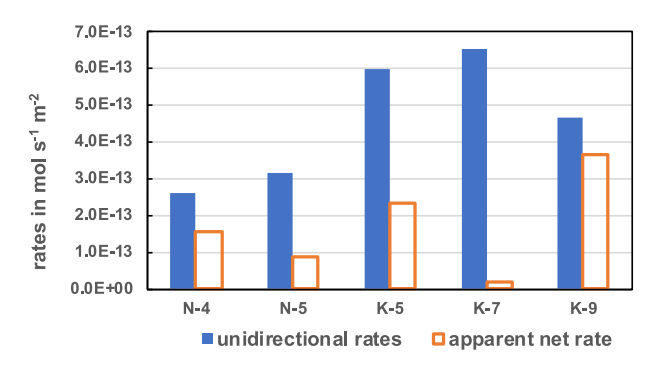


Fig. 10. Comparison of unidirectional dissolution rates derived from Si isotope ratios and apparent net dissolution rates from Si concentrations [Si]. The Si flux is the difference between Si release from feldspar dissolution and Si uptake by secondary phase precipitation. The Si isotope ratios in the experimental solutions changed only negligibly due to Si precipitation.

(Al inhibition effect) (Oelkers et al., 1994; Gautier et al., 1994). Future experiments should cover a range of departure from equilibrium under similar experimental conditions to make a better comparison.

Although our SI calculated for albite are near-zero, a numerical value near-zero can result from artifacts of thermodynamic data uncertainty and potential Al colloids in experimental solutions. A large range of  $\Delta_t G^{\circ}$  values for albite have been proposed (Arnórsson and Stefánsson, 1999). The  $\Delta_t G^{o}$  value we chose for speciation modeling from Holland and Powell (2011) was retrieved from hightemperature phase equilibrium data; it has not been tested whether it is consistent with the aqueous species thermodynamic database in SUPCRTBL. However, using thermodynamic databases that attempted to be internally consistent with solubility data (Tutolo et al., 2014; Miron et al., 2016) did not significantly change the calculated SI for albite. The Tutolo et al. (2014) thermodynamic database gave the average  $\Delta_r G$  /RT for albite at steady-state as -0.20 (0.54 kJ/mol). The Miron et al. (2016) thermodynamic database provided an average  $\Delta_r G/RT$  at a steadystate of -0.89 (-2.39 kJ/mol).

For K-feldspars, the structure and compositions of samples used for thermodynamic measurements vary to a larger degree than those for albite (Arnórsson and Stefánsson, 1999) and recommended  $\Delta_f G^o$  values differ by 20 kJ/mol. As noted in Section 3.9, speciation calculations showed supersaturation with an SI of +1.94, but K-feldspar was dissolving significantly. This is likely an artifact of  $\Delta_f G^o$  value variation of different K-feldspar samples. Our experimental data from K-feldspar experiments also showed more scattering than the albite experiments.

In the experiments, we used 0.22  $\mu$ m filters to separate solids from aqueous solutions, but Al colloids, if present, could pass the filter in our samples. Speciation calculations in Fig. 9 give some estimates. Our albite experimental solutions were supersaturated with respect to Al(OH)<sub>3</sub>(am). If the "true" dissolved [Al] were controlled by Al(OH)<sub>3</sub>(am), [Al] should be  $\sim$ 0.5 log units lower ([Al] change from  $\sim$ 10<sup>1</sup>  $\mu$ M to 10<sup>0.5</sup>  $\mu$ M). The SI of albite would change from 0 to  $\sim$ 0.5.  $\Delta_r G/RT$  would be  $\sim$ 1.15, still within the range of the near-equilibrium region (see Fig. 2). However, if dissolved [Al] were controlled by gibbsite, [Al] should be  $\sim$ 2.5 log units lower and  $\Delta_r G/RT$  would be  $\sim$ 5.6. For K-feldspar experiments, Al concentrations were close to amorphous Al(OH)<sub>3</sub> solubility (Fig. 9).

What is important in the experimental data is that the SI stayed constant for feldspars and secondary phases over a long time, signaling coupled primary mineral dissolution and secondary mineral precipitation in the experimental systems (Steefel and van Cappellen, 1990; Lasaga et al., 1994; Lasaga, 1998; Zhu et al., 2004; Ganor et al., 2007; Maher et al., 2009; Zhu et al., 2010). An analysis of the characteristics of such coupled systems was given by Lasaga (1998) for a hypothetical system. Zhu (2009) and Zhu et al. (2010) used reaction path modeling with full kinetic treatments of feldspar dissolution and secondary phase precipitation and interpreted their own experimental results and those from Alekseyev et al. (1997). In this study, similar reaction path modeling was carried out to quantitatively interpret the batch experiment data. Only forward feldspar dissolution was allowed in the model, but this was coupled with the precipitation of a phase with Si:Al ratio of  $\sim 2:1$ .

The results reiterate what has been learned about coupled reaction systems in previous studies (cited above). Slower precipitation of secondary phase(s) relative to the dissolution of the primary mineral led the system to a quasi-steady state. At the quasi-steady state, the ratios for dissolution and precipitation rates are fixed when the rates are expressed in units of mol s<sup>-1</sup> kgw<sup>-1</sup>, and the dissolution reaction proceeds at a fixed  $\Delta_r G$ . Some parameters were constant or changed slightly (e.g., [Al] and [Si]); others changed significantly (e.g., [Na]). The system was not at equilibrium and could not reach equilibrium because the coupled reactions "arrested" the system at a fixed SI or  $\Delta_r G$  level. The exact level of arrested  $\Delta_r G$  depends on the ratios of  $r'_{+,ab}/r'_{pre\cdotSi}$ .

#### 5.2. Artifacts of isotope exchange?

Could the measured slow dissolution rates from isotope tracer experiments be experimental artifacts? Isotope exchange, loosely defined here as the attachment and detachment of Si isotope atoms from feldspar surfaces without a net gain of Si in the solution, would artificially inflate the  $f_{28}$  and lead to apparent dissolution rates higher than the "true rates". Here the true rates are defined as the destruction of mineral structure that results in the release of Si atoms from mineral into solution. The possible effects of isotope exchange on rate determination are the change of isotope composition on the feldspar surface. The increase of  $^{29}$ Si and decrease of  $^{28}$ Si on feldspar surfaces resulting from "isotope exchange" will lead to artificially inflated rates if the Si isotope abundances of pristine feldspars are used for rate calculations (i.e.,  $f_{28,ab}$ ,  $f_{29,ab}$  in Eqs. (5) and (6)).

For example, if we assume that all <sup>29</sup>Si removed from the solution in the first five days of the experiment in N-5 are deposited on the albite surface, the albite surface would have <sup>28</sup>Si, <sup>29</sup>Si, and <sup>30</sup>Si fractional abundances of 0.8539, 0.1174, and 0.0287, respectively. Using this modified surface composition, a 16% faster rate would be derived. Therefore, isotope exchange cannot explain the apparent slow dissolution rates measured using isotope tracers at near-equilibrium and near-neutral pH experiments.

# 5.3. Did feldspar form in our experiments?

Did the reverse reaction occur in our experiments at 50 °C? The Si isotope method itself cannot distinguish reverse reaction from secondary phase precipitation. However, a possible indicator is Na concentrations. In Fig. 8, the lines are [Na $^+$ ] predicted from albite dissolution with rates fixed by Si isotope ratios (Fig. 4), without any adjustments. In other words, if significant albite and K-feldspar precipitation (reverse reaction) had occurred, we would see Na $^+$  and K $^+$  consumption and a much slower increase of [Na $^+$ ] and [K $^+$ ] with time at steady state. Therefore, the good agreement between predicted and measured alkali aqueous concentrations suggests that the reverse reaction of feldspar precipitation in the near-equilibrium, undersaturated solutions is insignificant at this temperature.

In low-temperature systems (e.g., <100 °C), the energetic barriers for the nucleation and precipitation of allophane, imogolite, and other amorphous and poorly crystalline phases are much lower than that for the reverse reaction of feldspar formation. Although authigenic feldspars can form at low temperatures during burial diagenesis, it appears that their growth is slow and requires silica concentrations that are near amorphous silica saturation (Kastner and Siever, 1979). This suggests that, unless the silica concentrations are unusually high, feldspar precipitation, and therefore equilibration, would take a very long time at low temperatures. In our experiments, Si concentrations and Al/Si ratios were far below amorphous silica saturation and feldspar stoichiometry, respectively.

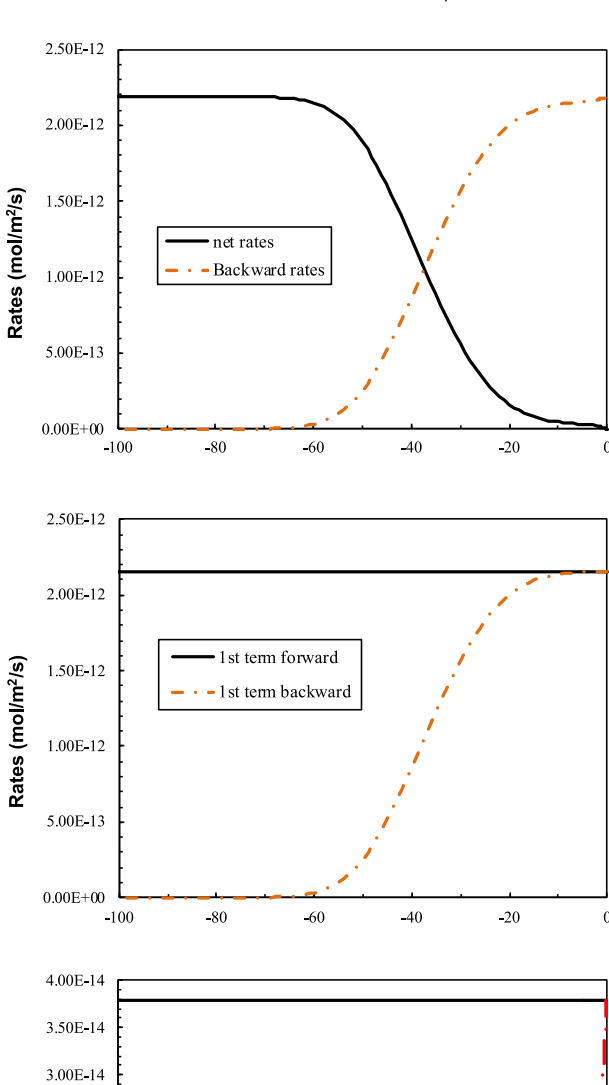
#### 5.4. Implications for geochemical modeling of weathering

The lack of significant reverse reaction in the near-equilibrium solutions found in this study has significant implications for geochemical modeling of weathering. Because experimental near-equilibrium rates are not available at weathering conditions, ambient temperature rates have been extrapolated from experimental data at hydrothermal temperatures. These extrapolations inherited the  $r_{\text{net}} = f(\Delta_r G)$  relationships that were established at high temperatures under which feldspar precipitation occurred.

For example, a common practice, due to a lack of alternatives—and that includes our own work—is to extrapolate the Burch type rate equation by Hellmann and Tisserand (2006) from 150 °C to 25 °C by calculating the rate constants  $k_1$  and  $k_2$  values at 25 °C through the apparent activation energies but the extrapolation retained the Burch type  $r_{\text{net}} = f(\Delta_r G)$  relationship established at 150 °C (Ganor et al., 2007; Yang and Steefel, 2008; Maher et al., 2009; Zhang et al., 2016). Fig. 11 deconstructs the Burch type rate equation (Eq. (5)) using the values of parameters listed in the figure caption. This equation, especially its first term, predicts high values of the backward reaction rate  $(r_{-})$  far away from equilibrium (i. e.  $r_{-}=r_{+}/2$  for  $\Delta_{r}G\sim$ - 40 kJ/mol). This occurs because the  $f(\Delta_r G)$  function in the first term of Eq. (5) implicitly accounts for the interruption of dissolution at etch pits by the development of the backward reaction which evidently is not the mechanism that stops etch pits nucleation.

Most geological systems are close to equilibrium. For example, White et al. (2001) studied the granite regolith in Georgia, USA. They found that soil and ground waters are close to equilibrium with respect to K-feldspar ( $\Delta_r G$  from -0.6 kJ/mol) to 0) and albite ( $\Delta_r G$  from -16.8 to -5.6 kJ/mol). Therefore, weathering models using far-from-equilibrium rate constants from compilations such as that of Palandri and Kharaka (2004) together with the Burch relation (Eq. (5)) or the classical TST rate law (Eq. (3)) simulate feldspar precipitation (an important backward reaction) for such soil water and groundwater systems.

In short, typically for reaction path and coupled reactive transport modeling, the model systems reach near-equilibrium within a short period of time. Using the  $r_{\text{net}} = f(\Delta_r G)$  relationship from high-temperature experiments or by incorporating Eq. (3), we were modeling the



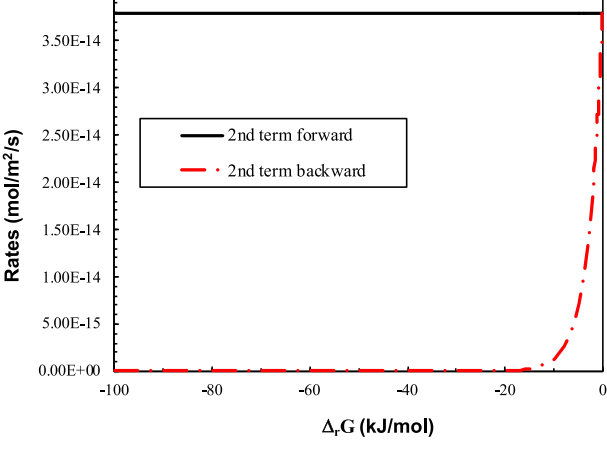


Fig. 11. A graph to illustrate the relationships among net rate  $(r_{net})$ , forward dissolution rate  $(r_+)$ , and reverse rate  $(r_-)$  as described in the Burch type rate equation proposed by Hellmann and Tisserand (2006).  $k_1$  in Eqn (5) of  $1.02 \times 10^{-8}$  mol s<sup>-1</sup> m<sup>-2</sup> measured at 150 °C was extrapolated to 25 °C via the Arrhenius equation using an apparent activation energy of 71 kJ/mol recommended for basic pH by Palandri and Kharaka (2004). The parameters that describe the  $r_{\rm net} = f(\Delta_r G)$  relationship at 150 °C was retained:  $n = 7.98 \times 10^{-5}$ ;  $m_1 = 3.81$ ;  $m_2 = 1.17$ . assumes significant feldspar precipitation (backward reaction). Applying this relationship to ambient temperature geochemical models predicts feldspar precipitation at these low temperatures.

reverse reactions of feldspar weathering at ambient temperatures, sometimes unknowingly.

# 5.5. A possible way forward for geochemical modeling of weathering

We recommend a different approach to model low-temperature and weathering systems (e.g., T < 100 °C). We should abandon the reliance on the  $r_{\rm net} = f(\Delta_r G)$  relationship to extrapolate from far-from-equilibrium to near-equilibrium rates. This study shows that the reverse reaction was negligible at low temperatures, which indicates that  $r_{\rm net} = f(\Delta_r G)$  relationships cannot be established experimentally at low temperatures.

Instead, we should use the newly available unidirectional forward rates at near-equilibrium, near-neutral pH conditions. Feldspar dissolution can be modeled by using the forward rate,  $r_+$ , in feldspar-undersaturated but close-to-equilibrium solutions as an irreversible reaction:

$$r_{+} = k_{+}S_{A} \quad \text{if } \Delta_{r}G < 0 \tag{8}$$

Here,  $k_+$  is measured under near-equilibrium conditions. (k+ values for feldspars and other silicates can be measured with the Si isotope tracer method at 25 °C or 4 °C). Table 6 below shows the recommended k+ values for albite and K-feldspar.

When Eq. (8) is coupled with secondary phase precipitation, the system will be arrested in a near-equilibrium region and the distance of departure from equilibrium determined by the slow precipitation rates of secondary phases (Steefel and van Cappellen, 1990; Zhu, 2009). Modelers have often found it necessary to disallow feldspar precipitation to simulate weathering systems when feldspar is supersaturated in soil waters (Godderis et al., 2010). This practice should be extended to the undersaturated region near-equilibrium.

For modeling secondary mineral growth, a separate equation from dissolution is recommended (Pham et al., 2011; Schott et al., 2012), for example, the BCF equation for net precipitation:

$$r_{net} = k_{BCF} (1 - \Omega)^2 \quad \text{if } \Delta_r G < 0 \tag{9}$$

where  $\Omega$  is the solution saturation state with respect to the secondary phase of interest. These equations can be easily implemented with minor modifications of geochemical modeling software or input files.

Solving Eqs. (8) and (9) together, even without an affinity term in Eqs. (8), the system of coupled dissolution and precipitation reactions will not go to equilibrium with respect to feldspars. Instead, the system will stay very close to equilibrium. Feldspar will continue to dissolve, and the secondary phase continues to precipitate until all feldspars in the system are exhausted.

For high temperature systems such as those described by Burch et al. (1993), Oelkers et al. (1994), Gautier et al., (1994), Alekseyev et al. (1997), Hellmann and Tisserand (2006), and Zhu et al. (2010), reverse reactions that form feldspars are possible, and an affinity term should be included in the rate law.

Table 6
Recommended forward reaction rate constants for modeling low-temperature systems in circumneutral pH.

	50 °C	25 °Ca	4 °C <sup>b</sup>
Kfs forward reaction rate, $k_{+}$ (mol feldspar m <sup>-2</sup> s <sup>-1</sup> )	$5.72 \times 10^{-13}$	$1.75 \times 10^{-13}$	$5.47 \times 10^{-14}$
Albite forward reaction rate, $k_{+}$ (mol feldspar m <sup>-2</sup> s <sup>-1</sup> )	$2.70 \times 10^{-13}$	$3.04 \times 10^{-14}$	$3.58 \times 10^{-15}$

<sup>&</sup>lt;sup>a</sup> Extrapolated via the Arrhenius equation using an apparent activation energy of 38 kJ/mol recommended for neutral pH by Palandri and Kharaka (2004).

The greatest challenge remains that the experimentally measured feldspar dissolution rates are orders of magnitude faster than those estimated from field systems (Paces, 1973; Velbel, 1985; White and Brantley, 2003; Zhu et al., 2004; Zhu, 2005). Extrapolated from 50 to 4 °C using an apparent activation energy of 70 kJ/mol from Palandri and Kharaka (2004), the albite unidirectional dissolution rate is on the order of 10<sup>-15</sup> mol s<sup>-1</sup> m<sup>-2</sup>, which is close to some field rates. These are laboratory determined rates on crushed and ground feldspar samples. It is possible that rates continue to decrease with reaction time (White and Brantley, 2003).

#### 6. CONCLUSIONS

Here we used the Si isotope tracer method for albite and K-feldspar hydrolysis experiments at 50 °C and pH 6.35–7.31 (neutral pH at 50 °C is about 6.6). The isotope tracer method allowed us to decouple the dissolution and precipitation rates in the near-equilibrium region. Unidirectional feldspar dissolution rates were obtained from isotope ratios. The decoupling revealed that the reverse reaction of feldspar formation does not occur at any significant rate at 50 °C. Instead, secondary Al-Si phases precipitated. The precipitation of secondary phases is coupled with feldspar dissolution and the coupled reactions keep the feldsparwater system "arrested" in systems in a steady-state very close to equilibrium for a long time.

These results of this study suggest that the establishment of overall rates of feldspar dissolution as a function of the departure from equilibrium  $(r_{\text{net}} = f(\Delta_r G))$  is not possible at near ambient temperature, given that the reverse reaction of feldspar dissolution—feldspar precipitation—is insignificant compared to the precipitation of Al-Si secondary phases. While such a relationship is desirable for extrapolating rates from far-from-equilibrium to near-equilibrium conditions, applying  $r_{\text{net}} = f(\Delta_r G \text{ established at high tem-}$ peratures, where feldspar precipitation can occur within laboratory experiment time, to ambient temperatures for modeling weathering is problematic. It would calculate feldspar precipitation in most soil and ground water systems, in which the aqueous solutions are near-equilibrium to but undersaturated with respect to feldspars. This is equivalent to saying that part of the soil is turning back to granite.

Given this situation, we recommend the use of unidirectional dissolution rates  $(r_+)$ , measured at conditions similar to natural systems (e.g., ambient temperature, near-equilibrium, near-neutral pH), and model feldspar weather-

ing as irreversible reactions. These rates can be obtained from Si isotope tracer experiments. Coupling the forward rate equation with the precipitation of secondary phase precipitation can be implemented by minor modifications of geochemical modeling software or input files.

#### 7. RESEARCH DATA

Research Data associated with this article can be access at https://doi.org/10.5967/v1mc-0736.

#### **Declaration of Competing Interest**

The authors declare that they have no known competing financial interests or personal relationships that could have appeared to influence the work reported in this paper.

#### ACKNOWLEDGMENTS

Discussions with Eric Oelkers, Carl Steefel, and Jim Kubicki, and comments from three anonymous reviewers have helped improve the clarity of the presentation. We are also grateful to Huifang Xu and Hiromi Konishi for their efforts to identify the secondary phases, Anne Hereford and Gregory H Zhu for editing, and Lei Gong for supervising the student experiments and managing the lab. This article is dedicated to the memory of our coauthor J. Don Rimstidt. Don passed away before this manuscript could be completed. He made a major contribution to this research, but sadly could not add his always valuable insights to the final manuscript and may not have agreed with all of our conclusions.

This work was partially supported by the U.S. NSF grant EAR-1926734 and the Faculty Research Support Program through the office of Vice Provost for Research at Indiana University to CZ. Analysis of Si isotopes was funded to HLY by the State Key Laboratory of Continental Dynamics.

### APPENDIX A. SUPPLEMENTARY MATERIAL

Supplementary data to this article can be found online at https://doi.org/10.1016/j.gca.2019.12.024.

#### REFERENCES

Alekseyev V. A., Medvedeva L. S., Prisyagina N. I., Meshalkin S. S. and Balabin A. I. (1997) Change in the dissolution rates of

<sup>&</sup>lt;sup>b</sup> Extrapolated via the Arrhenius equation using an apparent activation energy of 70 kJ/mol recommended for neutral pH by Palandri and Kharaka (2004).

- alkali feldspars as a result of secondary mineral precipitation and approach to equilibrium. *Geochim. Cosmochim. Acta* **61**, 1125–1142.
- Alekseyev V., Medvedeva L. and Bannykh L. (2004) Experimental and mathematical modeling of the kinetics of congruent and incongruent dissolution reactions of alkaline feldspars. Geochem. Int. CIC Geokhimiia 42, 848–861.
- Arnórsson S. and Stefánsson A. (1999) Assessment of feldspar solubility constants in water in the range of 0 to 350°C at vapor saturation pressures. *Am. J. Sci.* **299**, 173–209.
- Arvidson R. S. and Luttge A. (2010) Mineral dissolution kinetics as a function of distance from equilibrium - New experimental results. *Chem. Geol.* 269, 79–88.
- Beck J. W., Berndt M. E. and Seyfried, Jr, W. E. (1992) Application of isotopic doping techniques to evaluation of reaction kinetics and fluid/mineral distribution coefficients: An experimental study of calcite at elevated temperatures and pressures. Chem. Geol. 97, 125–144.
- Beig M. S. and Lüttge A. (2006) Albite dissolution kinetics as a function of distance from equilibrium: Implications for natural feldspar weathering. *Geochim. Cosmochim. Acta* 70, 1402–1420.
- Berger G., Beaufort D. and Lacharpagne J. C. (2002) Experimental dissolution of sanidine under hydrothermal conditions: Mechanism and rate. Am. J. Sci. 302, 663–685.
- Blum A. E. and Stillings L. L. (1995) Feldspar dissolution kinetics. In *Chemical Weathering Rates of Silicate Minerals* (eds. A. F. White and S. L. Brantley). Mineralogical Society of America, pp. 291–346.
- Brantley S. L. (2008) Kinetics of mineral dissolution. In *Kinetics of Water-Rock Interaction* (eds. S. L. Brantley, J. D. Kubicki and A. F. White). Springer, New York, pp. 151–210.
- Brantley S. L., Kubicki J. D. and White A. F. (2008) *Kinetics of Water-Rock Interaction*. Springer.
- Braunauer S., Emmett P. H. and Teller E. (1938) Adsorption of gases in mutlimolecular layers. *J. Am. Chem. Soc.* **60**, 309–319.
- Burch T. E., Nagy K. L. and Lasaga A. C. (1993) Free energy dependence of albite dissolution kinetics at 80° C and pH 8.8. *Chem. Geol.* **105**, 137–162.
- Chou L. and Wollast R. (1984) Study of the weathering of albite at room temperature and pressure with a fluidized bed reactor. *Geochim. Cosmochim. Acta* 48, 2205–2217.
- DePaolo D. J. (2011) Surface kinetic model for isotopic and trace element fractionation during precipitation of calcite from aqueous solutions. *Geochim. Cosmochim. Acta* 75, 1039–1056.
- Dove P. M., Han N. and De Yoreo J. J. (2005) Mechanisms of classical crystal growth theory explain quartz and silicate dissolution behavior. *Proc. Natl. Acad. Sci.* 102, 15357–15362.
- Drever J. I. (1988) The Geochemistry of Natural Waters: Surface and Groundwater Environment. Prentice-Hall, Englewood Cliffs, New Jersey.
- Eyring H. (1935) The activated complex in chemical reactions. *J. Chem. Phys.* **3**, 107–115.
- Gaillardet J. (2008) Isotope geochemistry as a tool for deciphering kinetics of water-rock interaction. In *Kinetics of Water-Rock Interaction* (eds. S. L. Brantley, J. D. Kubicki and A. F. White). Springer, New York.
- Ganor J., Lu P., Zheng Z. and Zhu C. (2007) Bridging the gap between laboratory measurements and field estimations of silicate weathering using simple calculations. *Environ. Geol.* 53, 599–610.
- Gautier J.-M., Oelkers E. H. and Schott J. (1994) Experimental study of K-feldspar dissolution rates as a function of chemical affinity at 150° C and pH 9. *Geochim. Cosmochim. Acta* 58, 4549–4560.
- Geisler T., Janssen A., Scheiter D., Stephan T., Berndt J. and Putnis A. (2010) Aqueous corrosion of borosilicate glass under

- acidic conditions: a new corrosion mechanism. *J. Non-Cryst. Solids* **356**, 1458–1465.
- Geisler T., Nagel T., Kilburn M. R., Janssen A., Icenhower J. P., Fonseca R. O., Grange M. and Nemchin A. A. (2015) The mechanism of borosilicate glass corrosion revisited. *Geochim. Cosmochim. Acta* 158, 112–129.
- Georg R. B., Reynolds B. C., Frank M. and Halliday A. N. (2006) New sample preparation techniques for the precise determination of the Si isotope composition of natural samples using MC-ICP-MS. *Chem. Geol.* 235, 95–104.
- Gin S., Jollivet P., Fournier M., Angeli F., Frugier P. and Charpentier T. (2015) Origin and consequences of silicate glass passivation by surface layers. *Nat. Commun.* **6**, 1–8.
- Godderis Y., Williams J. Z., Schott J., Pollard D. and Brantley S. L. (2010) Time evolution of the mineralogical composition of Mississippi Valley loess over the last 10 kyr: Climate and geochemical modeling. *Geochim. Cosmochim. Acta* 74, 6357– 6374.
- Gong L., Rimstidt J., Zhang Y., Chen K. and Zhu C. (2019) Unidirectional kaolinite dissolution rates at near-equilibrium and near-neutral pH conditions. Appl. Clay Sci. 182 105284.
- Govett G. (1961) Critical factors in the colorimetric determination of silica. *Anal. Chim. Acta* **25**, 69–80.
- Gruber C., Zhu C., Georg R. B., Zakon Y. and Ganor J. (2014) Resolving the gap between laboratory and field rates of feldspar weathering. *Geochim. Cosmochim. Acta* **147**, 90–106.
- Helgeson H. C., Murphy W. M. and Aagaard P. (1984) Thermodynamic and kinetic constraints on reaction rates among minerals and aqueous solutions II. Rate constants, effective surface area, and the hydrolysis of feldspar. *Geochim. Cosmochim. Acta* 48, 2405–2432.
- Hellmann R. and Tisserand D. (2006) Dissolution kinetics as a function of the Gibbs free energy of reaction: An experimental study based on albite feldspar. *Geochim. Cosmochim. Acta* **70**, 364–383.
- Holdren G. R. and Berner R. A. (1979) Mechanism of feldspar weathering-I. Experimental studies. *Geochim. Cosmochim. Acta* 43, 1161–1171.
- Holland T. and Powell R. (2011) An improved and extended internally consistent thermodynamic dataset for phases of petrological interest, involving a new equation of state for solids. *J. Metamorph. Geol.* **29**, 333–383.
- Kastner M. and Siever R. (1979) Low temperature feldspars in sedimentary rocks. *Am. J. Sci.* **279**, 435–479.
- Langmuir D. (1997) Aqueous Environmental Geochemistry. Prentice Hall, Upper Saddle River, New Jersey.
- Lasaga A. C. (1998) Kinetic Theory in the Earth Sciences. Princeton University Press, Princeton, New Jersey.
- Lasaga A. C. and Blum A. E. (1986) Surface chemistry, etch pits and mineral-water reactions. *Geochim. Cosmochim. Acta* 50, 2363–2379.
- Lasaga A. C., Soler J. M., Ganor J., Burch T. E. and Nagy K. L. (1994) Chemical weathering rate laws and global geochemical cycles. *Geochim. Cosmochim. Acta* 58, 2361–2386.
- Liu Z., Rimstidt J. D., Zhang Y. and Zhu C. (2016) A stable isotope doping method to test the range of applicability of detailed balance. Geochem. Perspect. Lett. 2, 78–86.
- Lu P., Fu Q., Seyfried, Jr., W. E., Hedges S. W., Soong Y., Jones K. and Zhu C. (2013) Coupled alkali feldspar dissolution and secondary mineral precipitation in batch systems: 2. New Experiments with Supercritical CO2 and Implications for Carbon Sequestration. Appl. Geochem. 30, 75–90.
- Lüttge A. (2006) Crystal dissolution kinetics and Gibbs free energy.
  J. Electron Spectrosc. Relat. Phenom. 150, 248–259.
- Maher K., Steefel C. I., White A. F. and Stonestrom D. A. (2009) The role of reaction affinity and seocndary mienrals in

- regulating chemical weathering rates at the Santa Cruz Soil Chronosequence, California. *Geochim. Cosmochim. Acta* 73, 2804–2831.
- Marini L. (2007) Geological Sequestration of Carbon Dioxide: Thermodynamics, Kinetics, and Reaction Path Modeling. Elsevier.
- Marty N. C., Claret F., Lassin A., Tremosa J., Blanc P., Madé B., Giffaut E., Cochepin B. and Tournassat C. (2015) A database of dissolution and precipitation rates for clay-rocks minerals. *Appl. Geochem.* **55**, 108–118.
- McBride M. B. (1994) *Environmental Chemistry of Soils*. Oxford University Press, New York.
- Melander L. (1960) *Isotope Effects on Reaction Rates*. The Ronald Press Company, New York.
- Melander L. and Saunders W. H. J. (1979) Reaction Rates of Isotope Molecules. John Wiley & Sons. New York.
- Miron G. D., Wagner T., Kulik D. A. and Heinrich C. A. (2016) Internally consistent thermodynamic data for aqueous species in the system Na–K–Al–Si–O–H–Cl. *Geochim. Cosmochim. Acta* 187, 41–78.
- Nagy K. L., Blum A. E. and Lasaga A. C. (1991) Dissolution and precipitation kinetics of kaolinite at 80° C and pH 3: the effect of deviation from equilibrium. Am. J. Sci. 291, 649–686.
- Oelkers E. H. and Schott J. (1995) Experimental study of anorthite dissolution and the relative mechanism of feldspar hydrolysis. *Geochim. Cosmochim. Acta* **59**, 5039–5053.
- Oelkers E. H., Schott J. and Devidal J. L. (1994) The effect of aluminum, pH, and chemical affinity on the rates of aluminosilicate dissolution reactions. *Geochim. Cosmochim. Acta* 58, 2011–2024.
- Ohlin C. A., Villa E. M., Rustad J. R. and Casey W. H. (2009) Dissolution of insulating oxide materials at the molecular scale. *Nat. Mater.* **9**, 11.
- Paces T. (1973) Steady-state kinetics and equilibrium between ground water and granitic rocks. *Geochim. Cosmochim. Acta* 37, 2641–2663
- Palandri, J.L., Kharaka, Y.K. (2004) A compilation of rate parameters of water-mineral interaction kinetics for application to geochemical modeling. US Geological Survey, Open File Report 2004-1068.
- Parkhurst, D.L. and Appelo, C. (2013) Description of input and examples for PHREEQC version 3—a computer program for speciation, batch-reaction, one-dimensional transport, and inverse geochemical calculations. US geological survey techniques and methods, book 6, 497.
- Pham V. T. H., Lu P., Aagaard P., Zhu C. and Hellevang H. (2011) On the potential of CO2-water-rock interactions for CO2 storage using a modified kinetic model. *Int. J. Greenhouse Gas Control* 5, 1002–1015.
- Pollet-Villard M., Daval D., Ackerer P., Saldi G. D., Wild B., Knauss K. G. and Fritz B. (2016) Does crystallographic anisotropy prevent the conventional treatment of aqueous mineral reactivity? A case study based on K-feldspar dissolution kinetics. *Geochim. Cosmochim. Acta* 190, 294–308.
- Rimstidt J. D. (2014) Geochemical Rate Models: An Introduction to Geochemical Kinetics. Cambridge University Press.
- Schott J. and Oelkers E. H. (1995) Dissolution and crystallization rates of silicate minerals as a function of chemical affinity. *Pure Appl. Chem.* 67, 903–910.
- Schott J., Oelkers E. H., Benezeth P., Godderis Y. and Francois L. (2012) Can accurate kinetic laws be created to describe chemical weathering?. C.R. Geosci. 344 568–585.
- Seimbille F., Zuddas P. and Michard G. (1998) Granite-hydrothermal interaction: a simultaneous estimation of the mineral dissolution rate based on the isotopic doping technique. *Earth Planet. Sci. Lett.* **157**, 183–191.

- Siivola, J., Schmid, R. (2007) List of Mineral Abbreviations. web site.
- Steefel C. I. and van Cappellen P. (1990) A new approach to modeling water-rock interaction: The role of precursors, nucleation, and Ostwald ripening. *Geochim. Cosmochim. Acta* 54, 2657–2677
- Stefansson A. (2001) Dissolution of primary minerals of basalt in natural waters: I. Calculation of mineral solubilities from 0 C to 350 C. *Chem. Geol.* **172**, 225–250.
- Stumm W. (1992) Chemistry of Solid-Water Interfaces: Processes at the Mineral-Water and Particle-Water Interface in Natural Systems, 1st ed. John Wiley & Sons, New York.
- Su C. and Harsh J. B. (1994) Gibbs free energies of formation at 298 K for imogolite and gibbsite from solubility measurements. *Geochim. Cosmochim. Acta* 58, 1667–1677.
- Su C. M. and Harsh J. B. (1998) Dissolution of allophane as a thermodynamically unstable solid in the presence of boehmite at elevated temperatures and equilibrium vapor pressures. *Soil Sci.* **163**, 299–312.
- Tutolo B. M., Kong X.-Z., Seyfried, Jr, W. E. and Saar M. O. (2014) Internal consistency in aqueous geochemical data revisited: Applications to the aluminum system. *Geochim. Cosmochim. Acta* 133, 216–234.
- Valle N., Verney-Carron A., Sterpenich J., Libourel G., Deloule E. and Jollivet P. (2010) Elemental and isotopic (Si-29 and O-18) tracing of glass alteration mechanisms. *Geochim. Cosmochim. Acta* 74, 3412–3431.
- Velbel M. A. (1985) Geochemical mass balances and weathering rates in forested watersheds of the southern Blue Ridge. Am. J. Sci. 285, 904–930.
- Verney-Carron A., Sessegolo L., Saheb M., Valle N., Ausset P., Losno R., Mangin D., Lombardo T., Chabas A. and Loisel C. (2017) Understanding the mechanisms of Si-K-Ca glass alteration using silicon isotopes. *Geochim. Cosmochim. Acta* 203, 404–421.
- Weiss D. J., Harris C., Maher K. and Bullen T. (2013) A Teaching Exercise To Introduce Stable Isotope Fractionation of Metals into Geochemistry Courses. J. Chem. Educ. 90, 1014–1017.
- White A. F. (1995) Chemical weathering of silicate minerals in soils. In *Chemical Weathering Rates of Silicate Minerals* (eds. A. F. White and S. L. Brantley). Mineralogical Society of America, pp. 407–458.
- White A. F. and Brantley S. L. (2003) The effect of time on the weathering of silicate minerals: why do weathering rates in the laboratory and field? *Chem. Geol.* **202**, 479–506.
- White A. F., Bullen T. D., Schulz M. S., Blum A. E., Huntington T. G. and Peters N. E. (2001) Differential rates of feldspar weathering in granitic regoliths. *Geochim. Cosmochim. Acta* 65, 847–869.
- Yang L. and Steefel C. I. (2008) Kaolinite dissolution and precipitation kinetics at 22°C and pH 4. Geochim. Cosmochim. Acta 72, 99–116.
- Zhang G., Lu P., Wei X. and Zhu C. (2016) Impacts of mineral reaction kinetics and regional groundwater flow on long-term CO2 fate at sleipner. *Energy Fuels* **30**, 4159–4180.
- Zhu C. (2005) In situ feldspar dissolution rates in an aquifer. Geochim. Cosmochim. Acta 69, 1435–1453.
- Zhu C. (2009) Geochemical Modeling of Reaction Paths and Geochemical Reaction Networks. In *Thermodynamics and Kinetics of Water-Rock Interaction* (eds. E. H. Oelkers and J. Schott). Mineralogical Society of America, pp. 533–569.
- Zhu C., Blum A. E. and Veblen D. R. (2004) Feldspar dissolution rates and clay precipitation in the Navajo aquifer at Black Mesa, Arizona, USA. In *Water-Rock Interaction* (eds. R. B. Wanty and R. R. I. Seal). A.A. Balkema, Saratoga Springs, New York, pp. 895–899.

- Zhu C., Liu Z., Zhang Y., Wang C., Schearer A., Zhang G., Georg R. B., Yuan H.-L. and Rimstidt J. D. (2016) Measuring silicate dissolution rates using Si isotope doping. *Chem. Geol.* 445, 146– 163
- Zhu C. and Lu P. (2009) Alkali feldspar dissolution and secondary mineral precipitation in batch systems: 3. Saturation states of product minerals and reaction paths. *Geochim. Cosmochim.* Acta 73, 3171–3200.
- Zhu C., Lu P., Zheng Z. and Ganor J. (2010) Coupled alkali feldspar dissolution and secondary mineral precipitation in batch systems: 4. Numerical modeling of kinetic reaction paths. *Geochim. Cosmochim. Acta* **74**, 3963–3983.
- Zimmer K., Zhang Y., Lu P., Chen Y., Zhang G., Dalkilic M. and Zhu C. (2016) SUPCRTBL: A revised and extended thermodynamic dataset and software package of SUPCRT92. *Comput. Geosci.* **90**(Part A), 97–111.
- Zuddas P., Seimbille F. and Michard G. (1995) Granite-fluid interaction at near-equilibrium conditions: experimental and theoretical constraints from Sr contents and isotopic ratios. *Chem. Geol.* 121, 145–154.

Associate editor: Carl Steefel